ALMA MATER STUDIORUM - UNIVERSITÀ DI BOLOGNA
CAMPUS DI CESENA
SCUOLA DI INGEGNERIA

CORSO DI LAUREA IN INGEGNERIA ELETTRONICA E
TELECOMUNICAZIONI PER L'ENERGIA

INITIAL ACCESS TECHNIQUES FOR 5G SYSTEMS

Elaborato in
Sistemi di Telecomunicazione LM

Relatore
Chiar.mo Prof. Ing.
DAVIDE DARDARI

Correlatori
Dott. Ing.
FRANCESCO GUIDI
Dott. Ing.
ANNA GUERRA

Presentata da
ELIA LEONI

Sessione III

Anno Accademico 2017-2018

Acronyms

4G fourth generation

5G fifth generation

IoT Internet of Things

SOTA state-of-the-art

gNB gNodeB

SA stand alone

NSA non stand alone

IA initial access

mmWave millimeter wave

massive-MIMO massive-multiple input multiple output

LTE long term evolution

BS base station

UE user equipment

BF beamforming

LOS line-of-sight

NLOS non-line-of-sight

PL path loss

RT ray tracing

PSS primary synchronization signal

TX transmitter

RX receiver

SNR signal-to-noise-ratio

PMD probability mass distribution

MLRI memory-less random illumination

SMBI statistic and memory-based illumination

EA exhaustive search

PDP power delay profile

GPS global positioning system

iBWS initial beam width selection

SLS sector level sweep

gSLS sector level sweep

D-SLS dynamic - sector level sweep

EDP enhanced discovery procedure

DB geo-located context database

ADd alternate direction discovery

ADdV alternate direction discrovery with variable beam-width

ADdS alternate direction discovery within a sector

ADdVS alternate direction discovery variable beam-width within a sector

ADdVS+ alternate direction discovery within a sector - extended

HetNet heterogeneous network

macro-BS macro cell base stations

SC-BS small cell base stations

HPBW half-power beamwidth

MLS memory less search

MBS memory based search

dBi decibels relative to isotropic radiator

Sommario

Nei prossimi anni è previsto un aumento del traffico dati, e la quinta generazione cellulare 5G dovrá fare affidamento su nuove tecnologie, come le onde millimetriche e il massive-MIMO, per soddisfare tale richiesta. Lo spettro di frequenze sotto i 6 GHz risulta infatti sovra-utilizzato, e le frequenze relative alle onde millimetriche promettono di garantire alte velocitá di trasmissione dei dati, grazie alla grande disponibilità di banda, specialmente attorno ai 60 GHz. Nonostante questo aspetto favorevole, si ha peró un elevato path loss e la difficoltá nel penetrare gli ostacoli. Per ovviare a tali problemi, l'utilizzo di tecniche di beamforming, ottenibili grazie all'uso congiunto di frequenze a onde millimetriche e massive-MIMO, permette di direzionare il pattern dell'antenna nelle direzioni spaziali desiderate, e di compensare il path loss grazie all'aumento della direttivitá.

Considerando un sistema cellulare 5G, una comunicazione di tipo direttivo impone che i beam dell'utente e della stazione radio base debbano essere allineati per garantire la comunicazione, introducendo possibili ritardi nella fase di accesso iniziale. Di conseguenza, lo studio di algoritmi adhoc, progettati per velocizzare questa fase rappresenta un sfida importante per l'ottimizzazione dei futuri sistemi 5G. Nell'ottica quindi di velocizzare l'accesso iniziale nelle reti 5G, in questa tesi prima di tutto mostriamo gli approcci proposti nello stato dell'arte, mettendo in evidenza gli aspetti che possono essere migliorati. Successivamente viene spiegato il simulatore che abbiamo implementato su Matlab, e infine viene introdotto un nuovo algoritmo. In particolare, l'algoritmo proposto si basa sulla memoria degli utenti visti per settore e sull'utilizzo di diverse configurazioni dei beam. Questi due aspetti combinati tra loro risultano innovativi rispetto allo stato dell'arte. I risultati numerici ottenuti dimostrano la bontà della tecnica proposta negli scenari 5G considerati.

Contents

Introduction

With a view to face the expected growth in capacity demand [1], the fifth generation (5G) of wireless mobile systems will adopt new technologies such as millimeter wave (mmWave) and massive-multiple input multiple output (massive-MIMO). Given the fact that, the spectrum under 6 GHz is fragmented and crowded, the mmWave frequencies promise to provide high data rates thanks to large chunks of untapped spectrum [2]. Nevertheless, the communication at such frequencies is not trivial due to the high propagation path loss (PL) and the sensitivity to blockage due to the presence of obstacles [3]. Therefore, the usage of beamforming techniques enabled by the joint use of mmWave and massive-MIMO, seems to be the main way to face the aforementioned propagation issues because directional communications provides beamforming gain which compensates the high PL and possibly enables spatial multiplexing thus increasing system data rate [3].

Considering a 5G cellular system, directional links usually need the alignment of the user equipment (UE) and base station (BS) beams, thus introducing possible delays in the initial access (IA) phase. In fact, upon entrance of a UE into a cell, the BS steers its beams in the whole angular space in order to find the UE. Since, whenever a UE enters within a cell it has to connect immediately to the network, the IA phase has to be fast. Moreover, due to the aforementioned blockage caused by the obstacles at mmWave, the IA at different BSs shall be repeated often at UE side. Thus, the study of ad-hoc algorithms designed to improve this phase represents one of the challenges for optimizing 5G systems. The IA algorithms can be classified in non stand alone (NSA) and stand alone (SA), depending on the joint use or not of a sub-6 GHz link (e.g. on long term evolution (LTE)) with the mmWave link, respectively. In this document, we first provide a review of the techniques proposed in the state-of-the-art (SOTA) for the IA procedure, then we present a Matlab simulator designed to test different algorithms in several scenarios (SA and NSA), and finally we introduce a novel algorithm to enhance the performance with respect to the SOTA approaches. The document is organized as follows: in chapter 1, after a brief introduction of the

IA phase, we provide a description of several SOTA algorithms. Our novel approach is described in chapter 2, focusing on both BS and UE side of the algorithm. The simulator we developed in Matlab with the purpose of testing the implemented algorithms is described in chapter 3. Finally, in chapter 4 we provide the numerical results obtained using our simulator and the main achievements are discussed.

Chapter 1

Initial Access in mmWave Cell

1.1 Introduction on 5G Systems

The 5G of wireless mobile systems is on the doorways. We expect a future where we will be surrounded by a pervasive presence of electronic devices connected to the web and capable of continuously interacting with us. Therefore, internet providers foresee to manage a larger number of devices operating at data rates at an unprecedented scale, that translates into an escalation of the required resources within the next years. Fig. 1.1 shows some examples of applications where the next 5G is expected to have a tremendous impact, by putting in evidence different challenges that have to be faced, such as high data speed and reliability, while guaranteeing an extremely low latency.

In order to address this ever increasing traffic demand, the large amount of available bandwidth above 10 GHz especially at mmWave frequencies (above 30 GHz) has the potential to greatly increase the capacity of fifth generation cellular wireless systems considering that the current LTE spectrum under 6 GHz is fragmented and crowded [2]. Nevertheless, a higher path loss is experienced at mmWave with respect to its counterpart in the lower microwave bandwidths. In addition, the blockage caused by obstacles could become an issue, due to the low capability of mmWave signals to penetrate materials [4]. Thus, the usage of small cells promises to provide higher bandwidth signal and extend coverage for more users. Small cells are low power, short range wireless transmission systems where BSs cover small geographical areas for indoor or outdoor applications [5].

Notably, the joint use of mmWave and massive array technologies allows to pack a large number of antennas (even hundreds) into a small area, thus enabling the possibility to integrate them into future portable devices. Several studies have been recently conducted towards this direction [6–8].

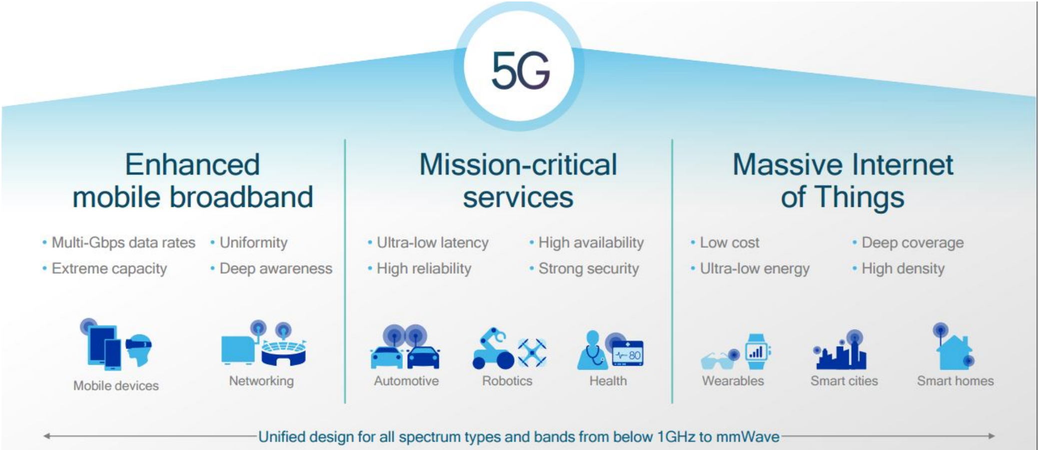

Figure 1.1: Example of several application fields with different requirements for the 5G [9].

Therefore, thanks to the possibility of realizing near-pencil beam antennas, accurate beamforming operations can be performed, allowing to focus the beam in very precise spatial directions and, thus, to avoid in part the aforementioned PL limitations.

Nevertheless, this spatial filtering also implies a different initial access to the cell: whenever a user enters a cell, it has to detect first the primary synchronization signal (PSS) transmitted by the BS and then to wait for a random access opportunity. After that phase a channel between the user and the network is set. This initial phase is called IA. Since the BS steers its beam in very precise spatial directions, the search by the UE of the PSS can become complex and lead to unsustainable delays also considering that due to obstacles such a phase could be repeated often. In the following, we first describe the IA procedure, and successively we report the SOTA on the current available techniques.

1.2 Introduction on Initial Access

In LTE systems, the UE is facilitated to obtain the time-frequency synchronization during the cell search phase, because the PSS is transmitted with an omni-directional or weakly directive antenna in the downlink, thanks to the low PL experienced in the microwave propagation, and beamforming is used only after a physical link has been established [2]. In the mmWave cell instead, the PSS is transmitted only in certain directions by the BS, which means that the UE's beam (if the UE does beamforming too) must scan

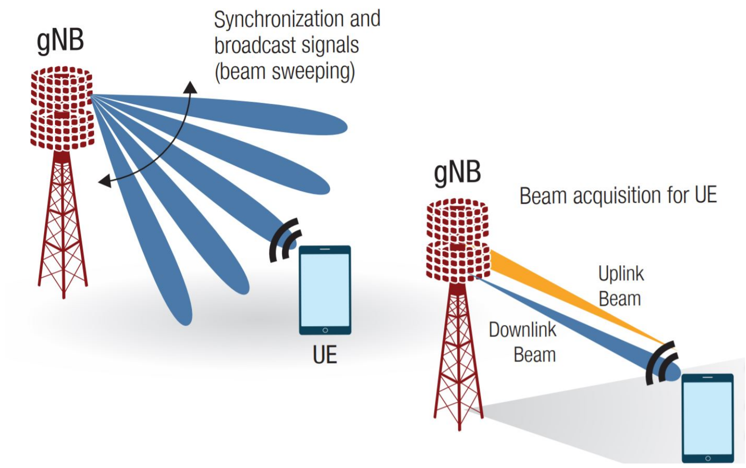

Figure 1.2: Initial Access in 5G. The BS is here named gNodeB (gNB) [10].

the whole angular space to search for the BS'beam and obtain the PSS to complete the access to the cell.

To be more specific, in every mobile communication systems, a terminal transitioning from IDLE to CONNECTED mode must perform the following steps [2]:

- *Cell Search*;
- *Random Access.*

The cell search is the phase which permits to an IDLE UE to find a suitable BS to connect with. In this stage the BS transmits the PSS in several discrete directions scanning the whole angular space, as shown in Fig. 1.2.

The UE has two options to detect the synchronization signal, according to its antenna: (i) by performing beamforming, in case it is equipped with an antenna array; (ii) or through an omnidirectional signal to explore the entire space. In this second scenario, the UE suffers for the high PL since it does not exploit the beamforming gain. On the other side, in (i) the UE needs to scan the entire angular space like the BS and thus the procedure is slower.

In our study we focus on the cell search described and in Chapter 2 we provide the description of an ad-hoc algorithm for optimizing this phase.

After the aforementioned step, the UE does not have a channel available to inform the network about its desire to establish a connection; the random access stage provides a mean to set up this connection. Both the UE and the BS know, from the previous phase, the directions through which they should steer their beams, and therefore they will exchange random access messages. After this step the UE is considered connected to the network.

The main problem of the previous stages, in particular of the first one, is that it must be very fast, because of the required low latency of the 5G network ($< 1\,\mathrm{ms}$). Moreover, due to the aforementioned blockage caused by the obstacles at mmWave, the IA at different BS shall be repeated often at UE side. Thus, it is very important to design a cell search algorithm which permits to create, when an UE enters the cell, a physical link between UE and the BS in the shortest possible time. Therefore, the *average discovery time*, that is, the mean duration of the IA phase, is a fundamental metric for the IA approaches, together with the misdetection probability i.e. the probability of detecting a UE once it enters within the cell.

Finally, the IA algorithms can be classified in SA and NSA approaches: SA identify an algorithm which does not rely on a sub-6 GHz link (e.g. on LTE), while in NSA a low frequency (with respect to mmWave frequencies) link is used as a control channel. NSA approaches might reduce the *average discovery time*, but since there must be a dedicated link for the control channel, this type of algorithms lead to a waste of resources. On the other hand, in the SA algorithms the IA operations are more complex, but they permit to deploy a complete 5G system since there is no need for LTE BSs.

1.3 State of the Art

In this Section, we provide a review of the main approaches adopted in the literature for IA in 5G *mmWave* cellular networks.

The table 1.3 shows several IA procedures. Every algorithm is described with six fields:

- *SA/NSA*;
- *Simulation Scenario*: this field indicates if authors have evaluated only line-of-sight (LOS) propagation or even non-line-of-sight (NLOS) propagation in the simulation phases;
- *Propagation Model*: this column shows if the considered propagation model is statistical (e.g. [11]), hybrid (e.g. [12]) or deterministic;
- *Memory*: an algorithm is considered with memory if takes into account the results of previous experiences. For example an algorithm which takes into account the number of users saw per sector;

Algorithm	SA/NSA	Simulation Scenario	Propagation Model	Memory	Context Information	UE transmission/reception type (BF or omni)
Exhaustive search (section 1.3.1)	SA	LOS	Model in [11]	No	No	BF
Iterative (section 1.3.1)	SA	LOS	Model in [11]	No	No	BF
Weigth-based search algorithm (section 1.3.2)	SA	LOS	Model in [11]	Yes	No	BF
MLRI (section 1.3.3)	SA	LOS	Model in [11]	No	No	BF
SMBI (section 1.3.3)	SA	LOS	Model in [11]	Yes	No	BF
Coordinated Initial Access (section 1.3.4)	SA	LOS	-	No	No	BF
iBWS (section 1.3.5)	NSA	LOS	Model in [11]	No	Yes	BF
gSLS (section 1.3.5)	NSA	LOS	Model in [11]	No	Yes	BF
D-SLS (section 1.3.5)	NSA	LOS	Model in [11]	No	Yes	BF
EDP (section 1.3.5)	NSA	LOS	Model in [11]	No	Yes	BF
Based on geo-located context Data Bases (section 1.3.6)	NSA	LOS/ NLOS	Hybrid model [12]/ One reflection RT [13]	Yes	Yes	BF
Alternate Direction Discovery Algorithms (section 1.3.7)	NSA	LOS	Hybrid model [12]/ One reflection RT [13]	No	Yes	BF
Multi base stations cell assignment (section 1.3.8)	NSA	LOS	Hybrid model [12]	No	Yes	OMNI

Table 1.1: Table containing a list of algorithms for the IA phase.

- *Context Information*: with context information we define the knowledge at the 5G BS of the users position, user orientation, user profiles, etc.., thanks to the aforementioned control channel;

- *UE transmission/reception type*: this field refers to the type of strategy at the UE side (i.e., omnidirectional vs beamforming).

1.3.1 Exhaustive and Iterative Approach

In [14], authors compare two algorithms, both consisting in a complete scan of the whole 360° angular space by the BS and the UEs in search for the best communication channel between them, according to fixed codebooks. More specifically, it is assumed a slot structure in which the PSS is periodically transmitted in each angular direction.

Exhaustive search performs a sequential beam searching: the BS has a predefined codebook of N directions (each identified by a beamfomring vector) that covers the whole angular space. While connecting a BS to a UE,

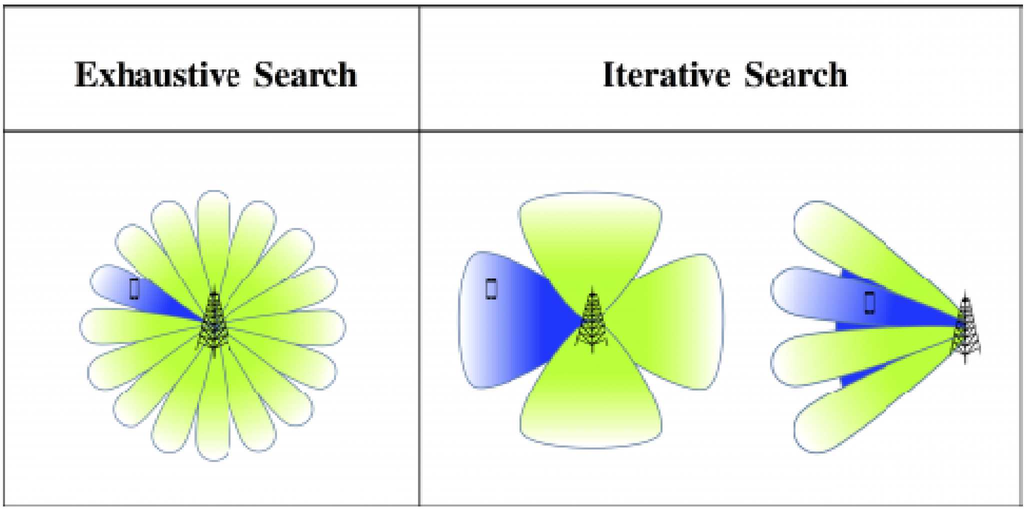

Figure 1.3: Comparison between Exhaustive and Iterative search [15].

the goal of this approach is to identify the best *transmitter (TX)-receiver (RX)* beam pair. Therefore, the BS sends messages in those N directions, in different slots, through narrow beams, while the UE configures its antenna array in order to directionally receive such messages. Upon the reception of a PSS, the UE evaluates the signal-to-noise-ratio (SNR) and, if it is above a pre-defined threshold, it sends back a PSS_{Rx} message to the BS. After having scanned the whole 360° angular space, the BS determines the best scanning direction to reach the UE, on the basis of the highest received SNR.

Iterative search performs a two-stage scanning of the angular space. Again, a codebook is available, in order to send synchronization messages in desired directions. In the first phase, the BS performs an exhaustive search through four macro wide beams and, after having scanned the whole 360° space, determines its best beam, on the basis of the highest received SNR (similarly the UE finds the best direction to reach the BS). In the second phase, the BS refines the search by performing a further exhaustive search, with a narrower beam, in the sector selected during the 1st phase. Fig. 1.3 shows the differences between the approaches.

Simulation Scenario

The BS is placed in the centre of a circular cell. At each iteration one UE is deployed according to a uniform distribution.

Simulation Results

In [14], it has been shown that the exhaustive approach ensures a lower misdetection probability than the iterative procedure but on the other hand the iterative one shows less *average discovery time* i.e. the time a BS needs to identify all users in its coverage range. Tests show that both algorithms present an acceptable midsedection probability for users in the range $0-30$ m. Therefore, when considering cells having very small radius, it may not be desirable to implement exhaustive search, because of its higher discovery delay. However, the iterative technique is not recommended when dealing with very dense networks because if multiple users are found in different macro directions, it is necessary to refine all of them, one at a time. Moreover, iterative technique shows bad performance even for *edge users* (95 meters from the BS).

1.3.2 Weight-Based Search Algorithm

The algorithm proposed in [16] accounts for the scan of the whole space like the aforementioned one, but in this case the order in which the sectors are scanned is based on the previous experience.

In this case the considered scenario consists in more UEs all around the BS. When the BS steers its beam in a particular sector and identifies one or more UEs (i.e. with SNR>threshold) it increases a counter, which is associated to the sector. Authors define a vector for storing and updating the counters related to each sector. When a scan of the overall space has been completed, the vector values are re-organized in descending order to establish how the new scanning will be performed, that is, giving more priority from the sector most populated to the least.

Simulation Scenario

The BS is placed in the centre of a circular cell. At each iteration one UE is deployed according to a uniform distribution.

Simulation Results

This algorithm shows less discovery delay than the exhaustive and iterative approach shown in previous subsection, due to the exploitation of the past attempts. Moreover, this improvement is obtained with performance, in terms of misdetection, close to the previous algorithms. Consequently, this approach enhance the aforementioned algorithms with a simple modification.

1.3.3 Memory-less Random Illumination and Memory-based Illumination

A statistical approach is proposed in [17] in order to minimize the mean discovery time of a user entered in a cell. The authors defines two probability mass distributions (PMDs):

- The probability p_i that a user enters from the ith sector;
- The entrance time probability w_k, with k indicating the index of the temporal slot (time is here divided into slots).

Fig. 1.4 shows an example of p_i considered by the authors. Both *memory-less random illumination (MLRI)* and *statistic and memory-based illumination (SMBI)* algorithms are based upon the a-priori knowledge of p_i and w_k.

MLRI considers the scan of the sectors with a probability q_i proportional to p_i without any update of the probability of entrance of the users. The equation in 1.1 shows the probability q_i:

$$q_i = \frac{1}{\sum_{j=1}^{N} \sqrt{\frac{p_j}{\epsilon_j}}} \sqrt{\frac{p_i}{\epsilon_i}} \tag{1.1}$$

where N is the number of sectors in which the space is divided. Moreover, the authors associates to the ith sector a detection probability ϵ_i, which takes into account errors in the discovery process due to effect of noise, channel fading and interference.

SMBI illuminates a certain sector in the time slot k based both on the statistics of users entrance (p_i and w_k) and on the fact that the user has not yet been discovered in the kth slot. They consider that the probability of finding the UE in slot k illuminating sector l is:

$$v_k(l) = \sum_{t=1}^{k} w_t \frac{p_l^{(t)}}{\sum_{i=1}^{N} p_i^{(t)}}, \tag{1.2}$$

where the probability that the UE is in sector l, $p_l^{(t)}$ is updated considering the previously illuminated sectors and the fact that it entered at time t, i.e.:

$$p_l^{(t)} = p_i \epsilon_i^{C(k,t,i)}, \tag{1.3}$$

where $C(k,t,i)$ represents the number of times that sector i has been illuminated between time t and k. Finally, they obtain a deterministic sequence to scan the whole angular space $\{b_k\}$ by computing:

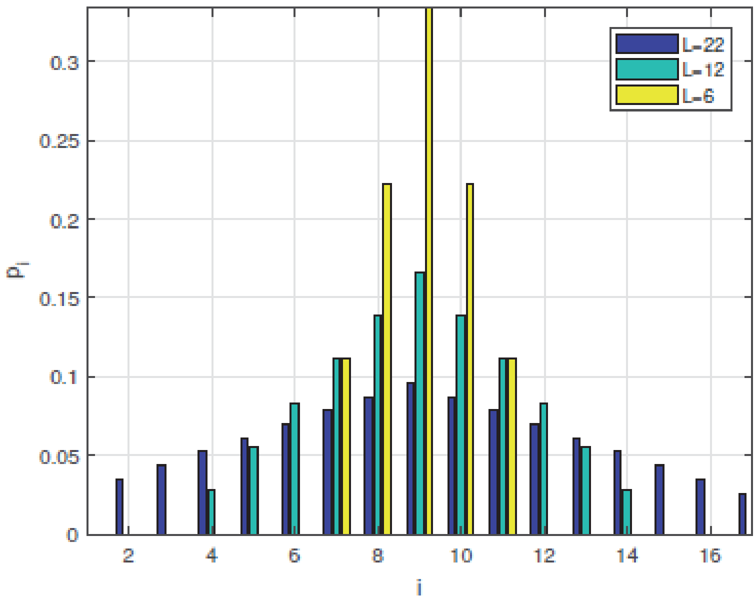

Figure 1.4: Example of sector entrance distribution p_i [17].

$$b_k = \underset{l}{\operatorname{argmax}}\, v_k(l). \tag{1.4}$$

This sequence is considered to scan the space as long as p_i and w_i do not change.

Simulation Scenario

The BS is placed in the centre of a circular cell. p_i (equilateral triangular PMD with parameter L shown in fig 1.4) and w_k (exponential distribution) are used to deploy users into the spatial sectors at a certain time slot, respectively.

Simulation Results

In [17], a comparison among MLRI, SMBI and exhaustive search is performed, by considering the *average discovery time* and the false alarm and misdetection probabilities as figures of merit to evaluate the performance. Notably, the *average discovery time* indicates the mean number of slots between the user entrance and its discovery by the BS after the IA procedure. Indeed, SMBI outperforms both exhaustive search (EA) and the

MLRI scheme in terms of misdetection probability by putting also in emphasis the need to carefully design the threshold to balance both the false alarm and the misdetection probability. Concerning the *average discovery time*, results show that MLRI algorithm does not significantly improve EA performance, due to the fact that it is based only on estimated p_i (it is possible that sectors are explored more than once in N consecutive slots), while SMBI outperforms both algorithms also in terms of *average discovery time* thanks to the exploitation of the memory.

1.3.4 Coordinated Initial Access

The solution proposed in [18] is based on the assumption that multiple BSs are allowed to coordinate each other by sharing the *power delay profile (PDP)* measurement reports via backhaul links in addition to the location and beam codebook information. This algorithm involves at least three mmWave BSs which cooperate to find the position of the UE supposed to be positioned inside the triangle whose vortexes are the BSs positions.

First, the UE transmits a known sequence through beams covering the whole 360° angular space as depicted in Fig. 1.5. For every UE beam, the BSs store in a database the PDP measure by steering their beams in random directions. After that the BSs share each other the PDPs and calculate an estimate of the angles between each BS and the UE. Therefore, thanks to the Carnot Theorem, this angles permit to evaluate the distances between every BS and the UE. After this operation, each BS is enabled to steer its beam towards the UE direction.

Simulation Scenario

The UE is generated into the triangle whose vertexes are the three BSs. Figure 1.5 shows the scenario.

Simulation Results

In [18], the proposed solution is compared with a similar approach but in absence of coordination between the BSs. Simulation shows that the *average discovery time* is reduced with the exploitation of the backhaul link between the BSs. Authors also claim that this type of algorithm could even deal with a NLOS case, thanks to the expected high density small cells deployment of the 5G i.e., at least three BSs are always in LOS with the UE.

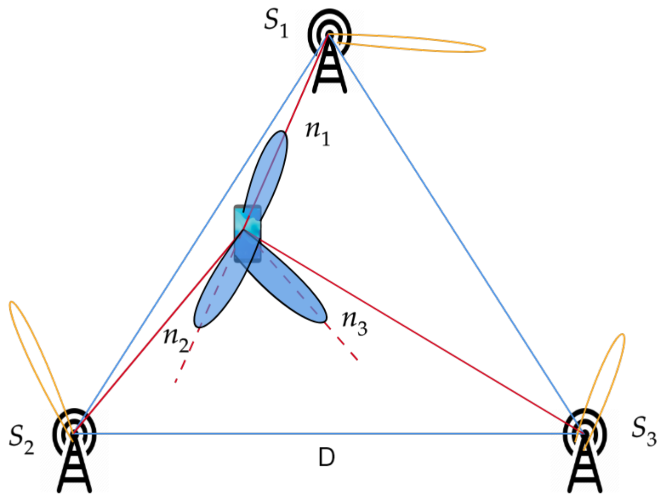

Figure 1.5: Scenario considered in [18].

1.3.5 Approaches Based on Context Information

Several algorithms using context information (in particular spatial position of each BS and UE through *global positioning system (GPS)* system) are defined in [13]. This subsection covers scenarios without obstacles whereas the effect of obstacles is investigated in the following section.

The awareness of the GPS coordinates of both BS and UE (by means of a low frequency control channel, i.e. an LTE connection) permits to point each others with a certain accuracy limited by the location error of the GPS. The location error is the principal problem for this type of algorithm. Indeed, if the user's position could be known with absolute certainty, BS and UE would be able to point each other immediately in an obstacle-free environment.

The first constraint accounted for in [13] is the scarce complexity affordable at the UE side. Consequently, a realistic solution cannot be much more complex than the sector level sweep (SLS) i.e. an exhaustive search. Given such a consideration, authors propose *initial beam width selection (iBWS)*, a procedure which processes the UE location and selects the best combination of beam widths at both BS and UE side. After that, they inform each other about what it has been selected through the separated control channel. The selection is based on the GPS coordinates of the UE, and it is useful to set the first direction and beam width for both the BS and the UE. There are three possible width combinations for the iBWS procedure:

- *Wide BS - Narrow UE (wBS - nUE)*: the one with the largest beam width at BS side;

- *Narrow BS - Wide UE (nBS - wUE)*: the one with the largest beam width at UE side;
- *Balanced*: the one with the minimum difference between the BS and the UE beam width.

After the aforementioned phase, three algorithms are proposed in order to extend the simple brute-force scanning of the sectors (i.e. *SLS*) at the BS side :

- *sector level sweep (gSLS)*;
- *dynamic - sector level sweep (D-SLS)*;
- *enhanced discovery procedure (EDP).*

gSLS is a straightforward extension of the SLS approach. It ignores iBWS and considers a fixed beam width which corresponds to the narrowest available value in order to preserve the largest coverage. The procedure starts by configuring the beam parameters pair at BS side (beam width and pointing direction) for the nominal user position, obtained from the control channel which knows the GPS position of the UE. Afterwards, if the user has not been found yet, the BS proceeds to circularly sweep through adjacent beams until the whole circle has been explored or until the UE has been detected. Users that cannot be discovered by this procedure are defined as unreachable.

D-SLS is a search paradigm that dynamically adapts beam widths. The search starts considering the beam with the width and the direction set by the iBWS strategy. If the user is not immediately detected, the mmWave BS sequentially scans around through every direction, keeping the same beam width. If no user is still found, the mmWave BS restarts the circular sweep with a reduced beam width. The following scanning operation considers a larger area (see Fig. 1.6-right) as well as a larger number of attempts. The procedure is repeated until every combination of beam width and pointing direction is explored.

EDP exploits the context information in a smarter way than the others algorithms. The search starts in the same way as for the D-SLS approach, but in this case if the user is not found within the first beam, the BS varies the beam width scanning n adjacent sectors (adjacent to the user position and $2\pi/n$ wide) in a clock-wise and counter clock-wise way. D-SLS and EDP are shown in Fig. 1.6.

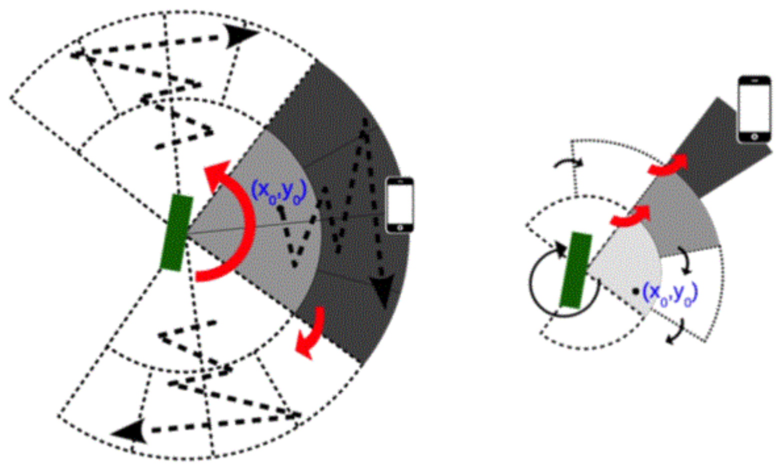

Figure 1.6: Left EDP, right D-SLS . Estimated user location is (x_0, y_0) [13].

Simulation Scenario

One BS is placed in the middle of a $450 \times 350\,\text{m}^2$ m area, while users (user's nominal positions i.e. the one indicated by the localization system) are dropped in this area according to a normal distribution centred in the BS with standard deviation σ_{pos}. The user-location uncertainty is modelled by considering the real user position distributed as a symmetric and independent bivariate normal distribution centred in the nominal position with parameter $\sigma_x = \sigma_y = \sigma$.

Simulation Results

The performance of the search strategies is first evaluated in terms of location error, without iBWS (at UE side a simple SLS strategy is assumed). In particular, it has been evidenced that EDP generally outperforms gSLS and D-SLS, especially for small location errors (i.e., less than 100 m). In addition, concerning the EDP strategy, the number of required steps might be reduced by increasing the number of adjacent sectors (i.e., n). On the contrary, the number of steps sharply increases when more sectors are used and the location error is large. Indeed, when the positioning error increases, the higher error sensitivity of narrower sectors negatively impacts on EDP performance: the algorithm gets caught in a deep exploration of a sector that could be wrong due to the position inaccuracy.

Authors evaluate the impact of the iBWS strategy in terms of *average discovery time*. They combine the aforementioned strategies with D-SLS and EDP search scheme, showing the performance as a function of the location error $\epsilon = 3\sigma$ in two cases which differ for the standard deviation of the normal distribution of the nominal positions is set:

- σ_{pos} =100 meters i.e. users on average more distant from the BS;
- σ_{pos} =10 meters i.e. users on average closer to the BS.

In the first case they prove that the iBWS strategy with wBS - nUE gives results similar to the aforementioned approach without iBWS, while nBS - wUE shows an improvement with respect to it, since the location error is low ($\epsilon < 80\,\mathrm{m}$ for EDP and $\epsilon < 30\,\mathrm{m}$ for D-SLS). On the other side, when UEs are closer to the BS, the iBWS strategy is very effective when the location error is small, leading the discovery phase to be very close to the remarkable result of establishing a BS-UE connection at the first attempt.

In [13], it is also proved that EDP generally outperforms D-SLS when the location error is small, while it degrades and becomes less convenient for larger errors. This is true for both aforementioned cases, but it is less evident when users are closer to the BS. Thus, it emerges that it is more favorable to explore the space in the angular domain, as happens in D-SLS.

1.3.6 Approaches Based on Geo-located Context Database

We now focus on the approach in [13], but for scenarios with the presence of obstacles. The knowledge of the GPS coordinates does not allow to find out the feasible steering directions at BS side for the NLOS UE. Therefore, authors claim that a practical approach could leverage on a geo-located context database (DB), useful to exploit reflected rays due to the quasi-perfect mirror behaviour of the surfaces in mmWave propagation [13].

The idea of using a DB is as follows (see Fig. 1.7). The system starts without the knowledge of where and when UEs can be detected. Then, once a new user is discovered the algorithm stores the correct beamforming configuration in the DB in terms of $[(x, y), w, d]$ where (x, y) is the user estimated position and w, d are respectively the width and the direction of the beam which can reach the user. Such information, which is collected also for the successive UEs, can be exploited to speed-up the IA process, by starting the search from the "known positions" that exhibited a higher presence of new UEs in the past attempts. Notably, in [13] only the beam parameters are stored, whereas the information on UE orientation is discarded. In fact, according to the authors' considerations, even small UE orientation errors can have a detrimental impact on the use of the previously collected data, thus limiting the beneficial effects.

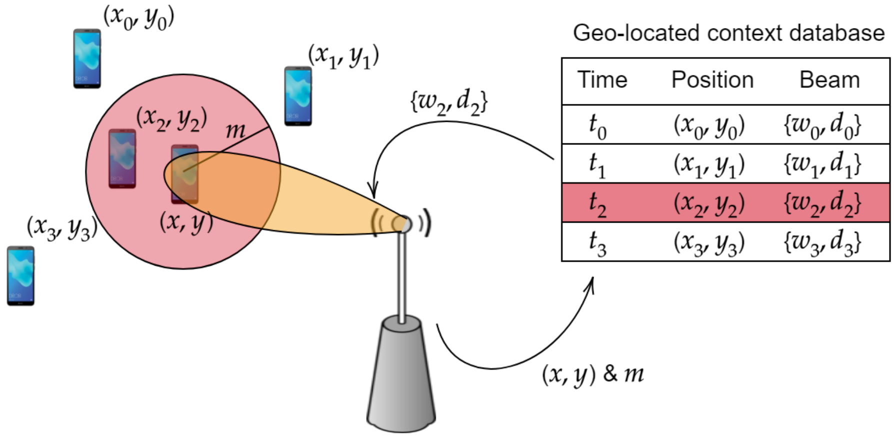

Figure 1.7: Example of range m setup in geo-located context database.

In order to better understand the function of the DB an important aspect is the concept of "closeness" to a position associated to a DB entry. To this aim, authors introduced a range m. Given a new user requesting access from a nominal position $p = (x', y')$, m indicates the maximum distance from p to delimit the search in the DB among the stored positions. Successively, the stored positions that are at a distance lower than m with respect to p, are first sorted starting from the closest one, and then tested to detect the UE. If the user is not found using DB information, the search proceeds by activating one of the algorithms proposed in the previous subsection.

Simulation Scenario

The scenario is the same as the previous subsection, but in this case obstacles are placed inside the area, generated with a uniform distribution for each simulated cycle. Obstacles have size $20 \times 20\,\mathrm{m}^2$, and they are considered as opaque bodies with reflecting edges. They assume the area boundary reflecting as well. Due to the 2-D characterization of the scenario, ground reflections are not considered in the ray tracing model, but are statically included in the propagation model in terms of random fading. The number of obstacles considered in the test phases is 0, 10 and 20.

Simulation Results

An important characteristic that must be discussed is the range m. Results obtained varying the location error prove that a too low value of m prevents the full exploitation of the DB: in fact only users very close to a DB entry can access the DB, even if the same information could be useful for more distant users. Vice versa, when the value of m is too large, many beams suggested by the DB become uncorrelated with the user location, thus leading to a wastage of unsuccessful beamforming attempts.

Authors also test the impact of the range m on the probability of success conditioned on that at least one candidate DB entry is available and considered for the incoming user. Tests put in evidence a trade-off between aspects. From one side, the increase of m implies that users "relatively far" from DB have in most cases "non-empty" candidate sets. This generally decreases the conditioned success probability because it might badly associate users with DB entries. However, increasing m enlarges the set of beam configurations that can be tested when the DB is accessed, thus increasing the success probability, especially in case of location errors.

1.3.7 Alternate Direction Discovery Algorithms

In [19], authors investigate a framework for mmWave initial access relying on contextual information which considers several advanced features. First, it is assumed that smart directional cell discovery algorithms can be applied to both BS and UE devices. Second, they claim that different context type and accuracy can be available in real implementations, therefore this information could be used to improve the IA performance.

To this aim they initially propose two algorithms which leverage on the information about user's position and orientation:

- alternate direction discovery (ADd)
- alternate direction discrovery with variable beam-width (ADdV)

ADd is a straightforward extension of SLS algorithm: once iBWS selects the proper beam-width for UE and BS, a set of beam pointing directions is defined at both devices. Each device evaluates the angular difference between every beam pointing directions and the estimated direction toward the other device. Then, beams are sorted by increasing angular difference to define the beam sequence for the discovery. The area surrounding the devices is scanned according to that sequence.

ADdV derives from the ADd algorithm previously described by adding the possibility to dynamically select beam-widths during the discovery: considering the beam-width selected by iBWS, ADdV scans all the surrounding area as ADd. If no connection is established, ADdV reduces the beam-width and iteratively scans the area with a larger set of pointing directions. Hence, allowing devices to increase their antenna gain, ADdV can recover from the situations in which the selection made by the iBWS procedure cannot guarantee the BS-UE communication.

These algorithms rely only on the user's position and user's information, therefore they propose three others algorithms, two for the UE and one for the BS which are based on the awareness of the user's position, user's orientation together with their error ϵ_l and ϵ_ϕ, respectively. In particular, it is shown that by assuming perfect knowledge of the BS orientation and position, the beam selected at UE side depends on both UE position and UE orientation errors, while the BS beam selection can be affected only by UE location error. Indeed, the UE orientation error can have a larger impact on the IA procedure since the UE reference system can be completely changed. To mitigate this effect, they propose the following improved approaches:

- alternate direction discovery within a sector (ADdS)
- alternate direction discovery variable beam-width within a sector (ADdVS)
- alternate direction discovery within a sector - extended (ADdVS+)

ADdS and ADdVS are improvements of ADd and ADdV respectively at the UE side. It is shown that the awareness of the orientation angle error at the UE side allows defining an angular sector S_ϕ wherein the direction towards the BS is most likely to be. Accordingly, the UE can focus the discovery within S_ϕ and avoid the activation of unsuccessful beams. Thus, the UE can reduce the number of beam attempts, and consequently the discovery duration

At the BS side they propose a more sophisticated approach, the ADdVS+ algorithm which is an extension of ADdV. They claim that the UE position accuracy allows to define an angular sector wherein UE is expected to be located. This sector points towards the UE position and extends in such a way the circle defining the UE position error is included within the two radii defining the sector. The area surrounding the BS is divided into several of these sectors and each sector is explored according to the ADdVS approach. If the first sector is scanned without a success, all adjacent sectors are alternately (clockwise and counter-clockwise) explored.

Simulation Scenario

In [19], it is considered a mmWave base station placed in the middle of a $450 \times 350\,\mathrm{m}^2$ area surrounded by reflecting walls. A different number of squared $20 \times 20\,\mathrm{m}^2$ size obstacles are randomly placed depending on the scenario, while UEs are randomly dropped according to a uniform distribution within the area; UEs orientation is randomly chosen.

The user-location uncertainty is modelled by considering the nominal UE position as a symmetric bivariate normal distribution centred in the real UE position with standard deviation $\rho_x = \rho_y = \rho$.

The BS's orientation is assumed to be perfectly known, while UE orientation error is modelled considering the estimated (nominal) UE orientation as a uniformly distributed random variable with mean value corresponding to the real UE orientation and variance equal to $\sigma_\phi^2/3$.

Simulation Results

The ADd and ADdV are initially tested in an obstacle-free scenario. Two performance metrices are considered: the *average discovery time* (evaluated in terms of antenna configuration switches at the UE side) and the achievable coverage (evaluated in terms of successful initial access).

Tests demonstrate that, by applying the same discovery algorithm at both BS and UE, ADd has a lower IA duration than ADdV, due to the fewer beam configuration probed. However, although the beam-width adaptation mechanism of ADdV increases the search duration, it augments the probability to successfully discovery the UE.

After these tests, scenarios with obstacles are considered. In brief, results show that the presence of obstacles reduces the performance of the considered algorithms. In particular, obstacles exacerbate the trade-off between success rate and discovery delay.

Finally, authors test the others search approaches in the scenario with and without obstacles. Results are obtained by activating ADdVS+ at BS side and several different algorithms at UE side. In absence of obstacles, it is evidenced that ADdS and ADdVS algorithms, thanks to the richer context information, are effective in speeding up the initial access duration by reducing the search space with respect to ADd andADdV, respectively. As the orientation accuracy decreases, the search space increases, hence ADdS and ADdVS performance gets closer to those attainable with ADd and ADdVS.

Moreover, in the scenario with obstacles, it has been demonstrated that the best configuration consists in ADdVS+ at the BS and ADdV at the UE side, since the use of ADdV could help at improving the performance in NLOS with respect to ADdS and ADdVS are limited by the reduced search space.

1.3.8 Multi Base Stations Cell Assignment

A multi base station approach is proposed in [20]. As in [13,19], authors rely on a heterogeneous network (HetNet) where there are both LTE BSs (macro cell base stations (macro-BS)) and 5G BS (small cell base stations (SC-BS)), and on the awareness of the position of the UE into the macro cell.

In the proposed search scheme, the UE is initially connected to the macro-BS. The macro-BS can select some local SC-BS that can potentially serve the UE. A SC-BS is to be selected according to the context information of the UE (i.e. location information provided by the GPS). When a SC-BS receives the command and the UE's location from the macro-BS, it starts to sweep the area by transmitting reference signal in different directions in an exhaustive way starting from the UE position provided by the GPS.

Thus, in [20] authors put particular emphasis on how the macro BS selects the SC-BS that can serve the UE in the best possible way. More specifically, the selection criteria is based upon the estimated received power at the UE, computable thanks to the knowledge of the estimated user's position and the known SC-BSs positions.

According to the collected measurements, the macro-BS selects the best SC-BS for the UE. Here the macro-BS is considered as the entity that collects all the measurements, perform signal processing and sends commands to SC-BS. In that sense, the macro-BS performs the role of the network coordinator.

In this context, authors propose an ad-hoc SC-BS selection scheme, expected to improve the current adopted approach.

In both approaches, the macro-BS initially estimates the location of the UE. In the traditional scheme, the macro-BS successively sorts SC-BSs according to the expected strength of their received signal in the estimated location of the UE.

The macro-BS starts by sending the estimated UE's location to the first SC-BS with also the command to transmit a reference signal towards the UE. After that, the SC-BS tunes its beam direction towards the location that has been estimated by the macro-BS and starts sweeping the surrounding area by adopting an exhaustive search.

If the selected SC-BS cannot reach the UE after a full beam search, the macro-BS selects and commands the next SC-BS in the candidates list. This process will continue until either the UE discovers an SC-BS or there is no SC-BS left to search the area. In the latter case, the macro-BS itself can be associated to the UE.

The main difference between the conventional and the proposed approach is the criterion for sorting the SC-BSs and selecting them. In the scheme proposed in [20], the SC-BSs are sorted according to the probability of detecting the UE. For the ith SC-BS authors define the probability $Pr_C^{(i)}$ as the probability that the UE is within the coverage area. This probability depends on the UE location measurements, the statistic of the estimation error, the position of the SC-BS and its coverage area. This probability is calculated as follows:

$$Pr_C^{(i)} = \int_{C_i} f_{\Psi_{\mathrm{UE}}}(\Psi)\mathrm{d}\Psi \tag{7}$$

where C_i is the coverage area of the ith SC-BS and $f_{\Psi_{\mathrm{UE}}}(\cdot)$ is the probability density function of the UE's position. C_i is defined as the area in which the received power from the SC-BS, is higher than a threshold. According to this definition, C_i results to be a circular area.

In the beginning of the proposed algorithm all available SC-BSs are considered candidates and the SC-BS with the highest $Pr_C^{(\cdot)}$ are initially selected in order to maximize the probability $Pr_{C|selected}^{(\cdot)}$ of detecting the UE. By considering the fact that previously selected SC-BSs could not reach the UE, the probability that the UE is reached by another SC-BS is calculated and considered as the SC-BS selection metric:

$$\mathrm{BS}_{\mathrm{selected}} = \arg\max_{\mathrm{BS}_i} Pr_{C|selected}^{(i)} \tag{9}$$

where the probability $Pr_{C|selected}^{(i)}$ is calculated as follows:

$$Pr_{C|selected}^{(i)} = \int_{C_i \cup C_{\mathrm{selected}}} f_{\Psi_{\mathrm{UE}}}(\Psi)\mathrm{d}\Psi \tag{10}$$

where $C_{selected}$ is the union of the coverage of all previously selected SC-BSs.

Simulation Scenario

In [20] authors consider a HetNet composed by a macro-BS and arbitrary number of SC-BSs of different types in random places within the macro cell area. Only LOS communication is considered.

In the simulation the UEs are generate once a time in the area. The UE's position $f_{\Psi_{\mathrm{UE}}}(\cdot)$, is a two-dimensional Normal distribution centred at the estimated position.

Simulation Results

In [20], the proposed scheme is compared to the conventional one in terms of probability that the best SC-BS is selected before any other SC-BSs (i.e.

it guarantees the best receive power at UE side), and in *average discovery time* i.e. the average number of scanning directions for cell assignment. In addition, it is also investigated when three SC-BSs simultaneously transmit the reference signal in ad-hoc directions in search of the UE.

Operating like this, it is demonstrated that the probability of finding the best BS degrades when the density of the SC-BSs increases, although the proposed scheme shows a better performance than the conventional one. Especially, the proposed scheme with 3 SC-BSs which transmit simultaneously, ensures the discovery of the best BS, that is, whenever the UE is detected by a group of three selected SC-BSs, the best BS is always among them and is discovered.

When the approaches are compared in terms of *average discovery time*, it emerges that the proposed scheme, with only one SC-BS searching for the UE, allows to reduce the number of transmissions of the 35% with respect to the conventional algorithm. If the number of SC-BSs is set to 3, that number is reduced of the 70%, thus guaranteeing a much faster IA procedure.

1.4 Conclusions

In the SOTA, algorithms based on both single and multi BS have been proposed. In this work, we are particularly interested on single BS approaches, which were proposed relying only on mmWave technology (SA) [14, 16, 17] or considering also LTE, low frequency dedicated channels or GPS (NSA) [13, 19]. Most part of the works inherent to SA IA use statistical channel evaluation in simple scenarios [11] and usually neglect the UE to improve the IA procedure [14,16,17]. Statistical channels do not allow to account for the position mobile user and the correlation between the channels in different positions determined by the geometry of the environment. Thus, deterministic models are preferable to test memory-based approaches. Moreover, SA algorithms which leverage on a memory-based system [16, 17] do not associate the memory to several half-power beamwidths (HPBWs) i.e. different beam configurations, as described in chapter 3.

Thus, our aim is to propose a new SA memory-based algorithm, tested with a deterministic channel model based on an ad-hoc ray tracing (RT) simulator.

The next chapter introduces the proposed novel approaches, while the chapter 3 shows how the IA simulator works. Finally in chapter 4 we show the obtained results.

Chapter 2

The Proposed IA Algorithm

This chapter shows in details our proposed IA technique. In the following, we describe how our novel algorithm is developed at the BS and UE side.

2.1 BS Side Implementation

The proposed algorithm at BS side consists in a SA approach which leverages on the possibility of adopting antenna array patterns with different HPBW. Moreover, the algorithm exploits the past experience in the scenario, that is, it is based on the creation of a database that accounts for the number of detected users according to the sector and the exploited HPBW.

The motivation behind the proposed method is to reduce the scanning time duration in the IA procedure, to permit the BS to detect the presence of a UE in the shortest possible time, while guaranteeing a reliable misdetection probability. This aspect is important in the perspective of achieving low latency networks in next 5G. Hence, the possibility to learn from previous experience is fundamental for the next generation BS to achieve a faster IA phase. To improve the IA procedure, large beams are usually preferred because they permit to scan the area in a shorter time, since the number of sectors forming the whole angular space decreases with the increase of the HPBW, i.e. the width of the single sector. On the other hand, a larger beam usually implies a reduction in the antenna gain, so that the link budget between the UE and the BS worsen, and thus UEs might not be detected.

First we rely on the possibility for the BS to have several beam configurations available. Fig. 2.1 shows different possible beams.

Second, the BS can leverage on a *knowledge database* which takes the form of a table, that includes information about the detected UEs per sector with the adopted HPBW. Fig. 2.2 shows an example of the table. The rows

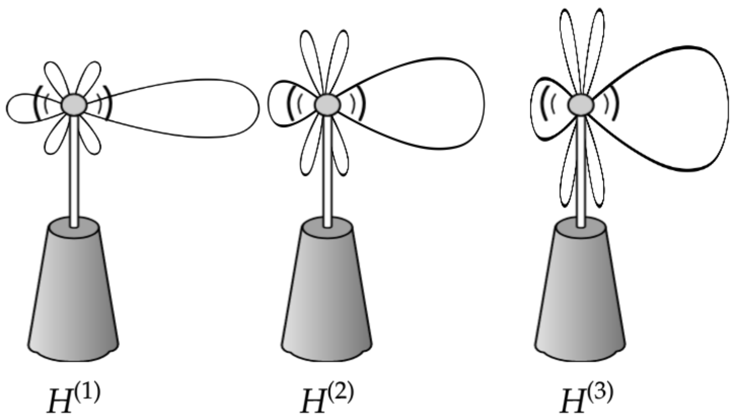

Figure 2.1: Example of three beams with different HPBW $H^{(1)}$, $H^{(2)}$, $H^{(3)}$.

of the matrix are as many as the number of considered HPBW, N_{Beam}. The columns instead correspond to a discretization of the whole angular space. For example a beam with a HPBW of 30° divides the whole angular space in 12 sectors. The discretization step is fixed by the beam with the minimum HPBW, $H^{(N_{Beam})}$, thus there are $N_{Sect} = \left\lceil \frac{360°}{H^{(N_{Beam})}} \right\rceil$ columns. Each cell in the matrix is an incremental counter. Notably, as it will be detailed in the following (see Fig. 2.4), specific ensembles of cells will form a tile.

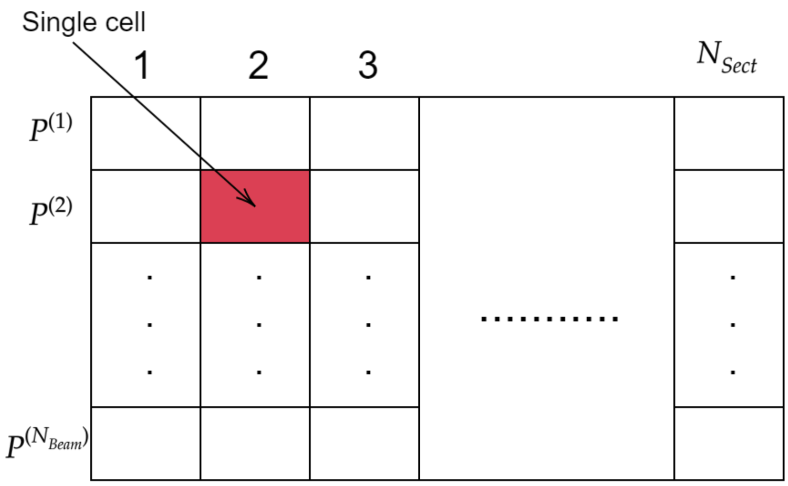

Figure 2.2: Example of *knowledge database*.

For sake of clarity, we define:

$$\mathbf{H} = \left[H^{(1)}, \dots, H^{(j)}, \dots H^{(N_{Beam})}\right]; \tag{2.1}$$

$$\mathbf{C} = \left[C^{(1)}, \dots, C^{(j)}, \dots C^{(N_{Beam})}\right]; \tag{2.2}$$

$$\mathbf{P} = \left[P^{(1)}, \dots, P^{(j)}, \dots, P^{(N_{Beam})}\right]; \tag{2.3}$$

$$H^{(j)} \iff \mathbf{S}^{(j)} = \left[S_1^{(j)}, \dots, S_k^{(j)}, \dots, S_{N_j}^{(j)}\right]; \tag{2.4}$$

$$C^{(j)} \iff \mathbf{T}^{(j)} = \left[T_1^{(j)}, \dots, T_k^{(j)}, \dots, T_{N_j}^{(j)}\right]. \tag{2.5}$$

where:

- $N_j = \left\lceil \frac{360°}{H^{(j)}} \right\rceil$;
- $\mathbf{H}$ is a vector containing the considered HPBW from the wider to the thinner;
- $\mathbf{C}$ is a vector containing the configurations of the beams, that is, the representation of the beam widths in the matrix;
- $\mathbf{P}$ is a vector where the jth element $P^{(j)}$ represents the maximum power level detectable with the HPBW $H^{(j)}$. Since, $P^{(1)} < \dots < P^{(j)} < \dots < P^{(N_{Beam})}$, $H^{(j)}$ allows to detect every user with a received power less than or equal to $P^{(j)}$. Each $P^{(j)}$ corresponds to a row in the matrix. Fig. 2.3 shows the beam widths and the corresponding maximum detectable power levels;
- The equivalence in Eq. 2.4 shows the correspondence between the jth HPBW and the jth vector of steering directions $\mathbf{S}^{(j)}$;
- The equivalence in Eq. 2.5 shows the correspondence between the jth configuration $C^{(j)}$ and the jth vector of tiles $\mathbf{T}^{(j)}$. The index j fixes the shape of the tile while k defines the position of the tile in the matrix;
- With $(H^{(j)}, S_k^{(j)})$ we define the couple HPBW, kth steering direction;
- With $(C^{(j)}, T_k^{(j)})$ we define the couple configuration, kth tile in the matrix.

Fig. 2.4 shows the examples of correspondence between the couples $(H^{(j)}, S_k^{(j)})$ and $(C^{(j)}, T_k^{(j)})$: for example the couple $(C^{(1)}, T_1^{(1)})$ in the table is equivalent to the couple $(H^{(1)}, S_1^{(1)})$ in the angular space. Thus, each direction of steering $S_k^{(j)}$ corresponds to a deviation of the beam in the azimuthal space, and

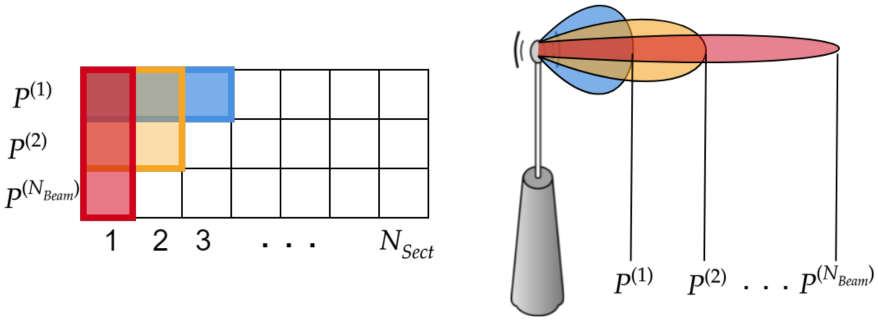

Figure 2.3: Example of several beams with different maximum detectable power levels. The matrix shows the tiles correspondent to the beams.

also indicates in the matrix the tile $T_k^{(j)}$. Each configuration moves along the columns by a step equal to its length in terms of columns.

Since each jth element $H^{(j)}$ divides the whole angular space in N_j sectors, each $H^{(j)}$ corresponds to a different vector $\mathbf{S}^{(j)}$. Hence, it is exactly the same for $C^{(j)}$ and the vector $\mathbf{T}^{(j)}$.
The *knowledge database* takes into account the number of UEs saw with the couples $(H^{(j)}, S_k^{(j)})$. Every time a UE is detected with a beam defined by a HPBW and a steering direction, the cells in the matrix correspondent to the couple $(C^{(j)}, T_k^{(j)})$ are incremented by one.

Whereby, it is possible to exploit this memory to privilege the beams with a HPBW and a direction such as they have detected more users during the functioning of the algorithm.

In order to do this we designed a simple iterative algorithm which tests every possible couple $(C^{(j)}, T_k^{(j)})$ in the matrix, and counts how many users each couples contain.

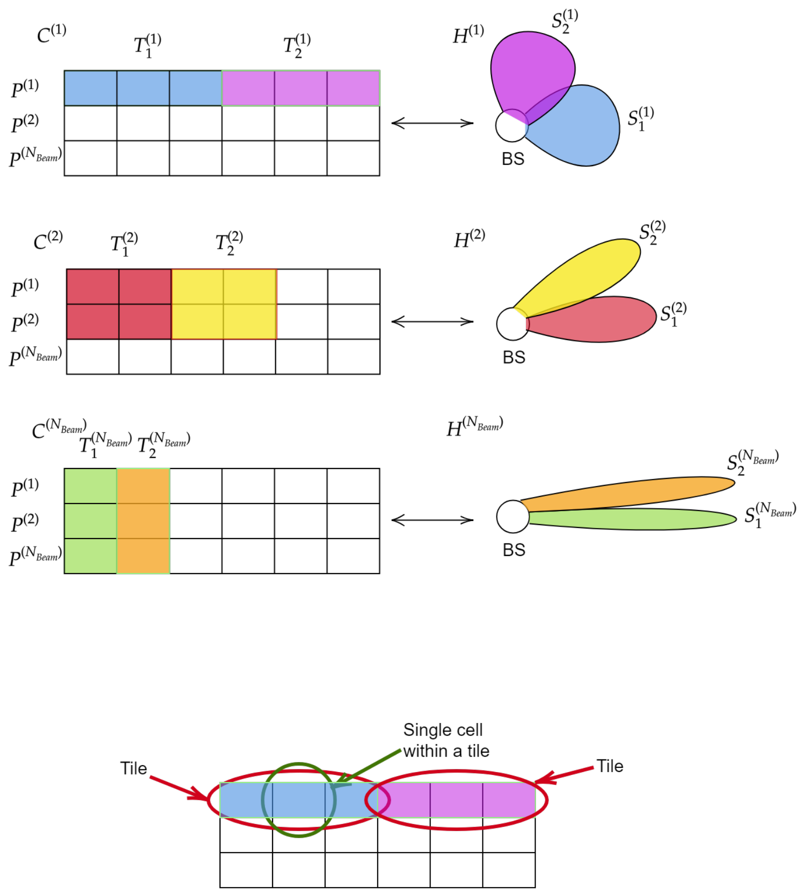

Figure 2.4: Top: example of equivalence between the couples $(H^{(j)}, S_k^{(j)})$ and $(C^{(j)}, T_k^{(j)})$. From $S_1^{(1)}$ to $S_1^{(N_{Beam})}$ the beam is shrinking. Bottom: definition of the tile and the cell within the tile.

At each iteration, the algorithm does the following steps:

1. Fixes a couple $(C^{(j)}, T_k^{(j)})$;

2. Sums the number of UEs inside the cells of the tile;

3. Saves this sum in a vector $\mathbf{X}$;

4. If the configuration $C^{(j)}$ has been checked for every $T_k^{(j)}$, tries the next configuration, otherwise it tries the next tile. In both cases it restarts from 1. Once every combination of $(C^{(j)}, T_k^{(j)})$ has been tested it passes to the next step;

5. Rearranges the vector $\mathbf{X}$ in descent order and uses the obtained order to create a sequence of couple $(H^{(j)}, S_k^{(j)})$. This sequence represents the order in which the couples $(H^{(j)}, S_k^{(j)})$ are to be tested to find a new UE.

Initially the matrix is empty, thus once the first UE enters within the cell the BS tests the couples $(H^{(j)}, S_k^{(j)})$ in a-priori defined order. Once the UE is detected by the BS with a certain $(H^{(j)}, S_k^{(j)})$, the correspondent couple $(C^{(j)}, T_k^{(j)})$ is incremented by one in the table.

Considering a fully operational situation, which means that the BS has already filled the table, here we provide the main steps of the algorithm when a new UE enters the cell:

- First of all the table is scanned as explained before. At the end of this operation a sequence of $(H^{(j)}, S_k^{(j)})$ is obtained;
- The BS scans the space following the aforementioned sequence in search of the UE;
- If the BS detects the UE with a certain $(H^{(j)}, S_k^{(j)})$, the cells in the table corresponding to the couple $(C^{(j)}, T_k^{(j)})$ are incremented by one.

The implementation and the results obtained with this approach are discussed in the chapters 3 and 4 respectively.

2.2 UE Side Implementation

According to the SOTA, the UE is not always equipped with an antenna array, but often with an omnidirectional antenna [20]. According to the considerations reported in chapter 1, when the UE is assumed to be equipped with an antenna array, only approaches with a rather low complexity have been exploited [13, 14, 19].

To improve current SOTA, in our method we assume that the UE takes advantage from three pieces of information: (i) the position deriving from the GPS; (ii) the experience of previous users, shared in a common repository (e.g., cloud), where the sector index, HPBW, etc. are stored once the detection is performed; (iii) the orientation, provided by internal sensors, so that it is possible correct the beamsteering weights according to the reference plane (apart from an error that will be discussed in Sec. 4.5).

Indeed, the information on the UE orientation helps at defining a unique reference system for the beamsteering operation, so that each user in the cell knows which is the correct beamforming configuration in order to point to the desired direction, unless an error due to its sensors.

Since the UE needs to integrate low complexity technologies, we consider that it is capable to steer its beam only in few different directions, thus dividing the whole angular space in sectors, as reported in Fig. 2.5.

Figure 2.5: Sectors at UE side.

The main idea behind the algorithm is the sharing of the information between mobile users that have experienced the same position so far. In particular, whenever a UE is detected in a certain cell, it saves in an online *database* its position, given for example by the GPS, and the beam direction adopted for successfully performing the IA procedure. In this way, the UEs that will successively enter in the same cell, will take advantage by the available data that derives from the past UEs experiences. In fact, each user is expected to access the information stored in the *database*, so that it knows which is the most favorable absolute steering direction for pointing towards the BS in its position.

This *database* is organized as shown in Fig. 2.6. The rows correspond to the previous UEs, where N_{UE} is the overall number of past UEs. The columns correspond to the 3D GPS coordinates and the others information (HPBW, sector, orientation etc..).

Nevertheless, using the *database* it is not straightforward. The information in the *database* is useful only if the new UE in the cell can leverage on the information of the closer past UEs. The behaviour of further past user could be very different from the behaviour of the new UE. To this aim we introduce the range R. This parameter defines if an entry in the *database* has to be considered or not. Fig. 2.7 shows an example of usage of the range R. In the example UE_1 and UE_2 are considered near to the new UE_{new}, while UE_3 is farther. Hence only UE_1 and UE_2 information has to be considered in the *database*.

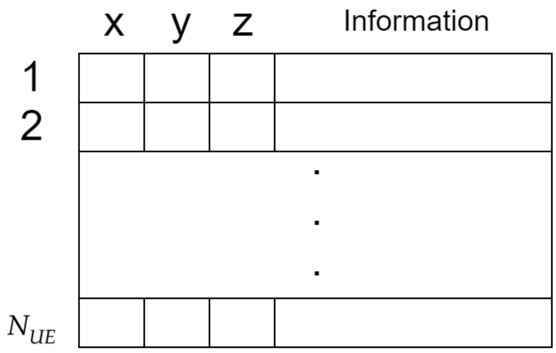

Figure 2.6: *Database* for the UE side of the algorithm.

Thus, for what the UE is concerned, the algorithm is organized as follows:

- A UE enters within a 5G cell;
- It controls the previously downloaded *database*;
- It corrects its beamforming weights according to the reference plane i.e., it converts the absolute direction (sector) stored in the *database* into relative direction (sector) according to its reference system of coordinates (reference plane) using its local inertial sensors;
- The UE orders its steering direction from the most usage to the least considering the directions used by the past UEs within the range R;
- The UE steers its beams in search for the BS;
- If the UE detects the BS it saves in the *database* its GPS position and its steering direction in which it found the BS.

The figure 2.8 shows how the algorithm should work.

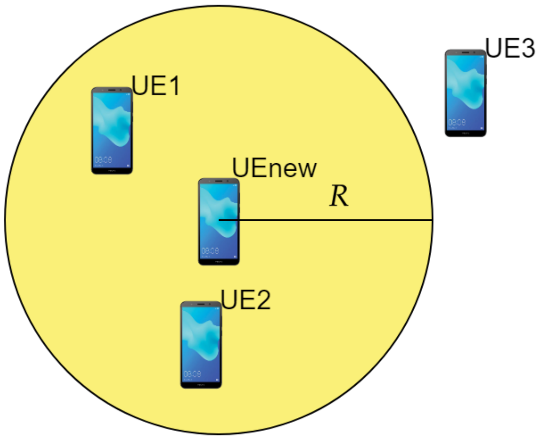

Figure 2.7: Example of range R. Each users within the circle defined by R is considered near the new user.

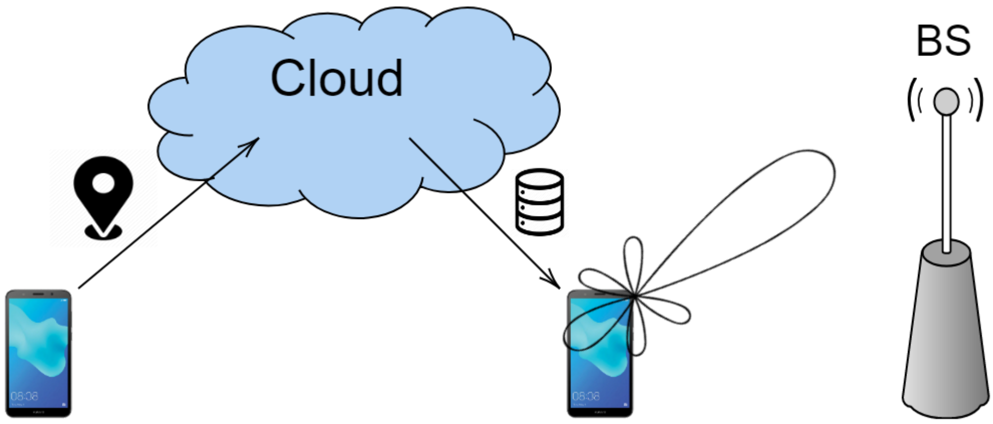

Figure 2.8: Acquisition and usage of the *database*. Thanks to the sharing of the information in the cloud the users could steers them beam immediately toward the BS.

Chapter 3

Initial Access Simulator

This chapter describes the blocks developed in Matlab for testing IA techniques for 5G, as depicted in the flowchart reported in 3.1. The four steps of the simulator will be described in the following sections, whereas the performance achieved with the algorithms, will be extensively investigated in the last chapters.
Thus, in the following we will introduce:

- *Scenario Generation*;
- *BSs and UEs Generation*;
- *Channel Model*;
- *Implemented Algorithms.*

3.1 Scenario Generation

First we introduce how the scenario containing the BS and the UEs is generated. Here there are two scenarios of interest:

- *Random geometry*;
- *Fixed geometry.*

The first one (similar to the one described in [13]) consists of a rectangle area, whose size is a-priori decided, and where obstacles are randomly generated with variable dimension. For the sake of simplicity, each obstacle is here intended as a square with variable area, and it is assumed to be an opaque body with reflecting edges (this point will be clarified in the channel

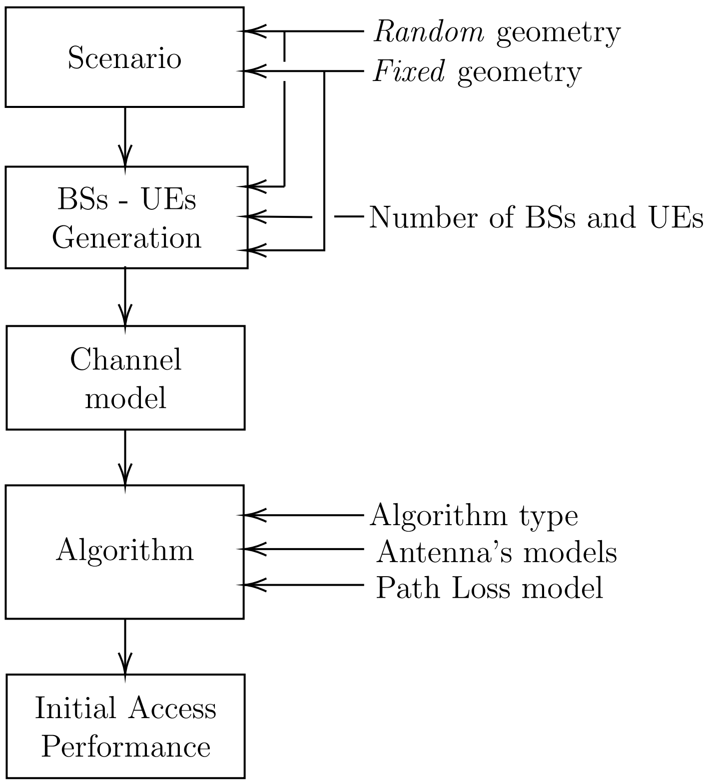

Figure 3.1: Flowchart of the simulator.

section 3.3). An example of generation of such a scenario is reported in 3.4, that shows the rectangle area with 20 obstacles inside.

This kind of scenario is useful to emulate for example a cell in a city, where users appear randomly located because they exit from the houses or because they switch on the mobile phone inside the cell. Fig. 3.2 shows a possible real scenario similar to the simulated one.

The second scenario reproduces a street-like environment where the number of obstacles, here representing possible houses close to the street, are varied from 0 to 4. Notably, due to the presence of the street, obstacles are here placed in a deterministic way i.e. their position are a-priori defined. Fig. 3.5 and 3.6 show two examples with 0 and 4 obstacles, respectively.

This particular scenario permits to investigate how IA techniques work where users enter the cell only from certain directions, because for example the BS is positioned beside a street. Figure 3.3 shows an example of cell, where the BS is placed close to the street and there are only 2 possible ways to enter the cell (indicated by the black arrows).

Dwelling on this type of scenario, it is straightforward to consider that

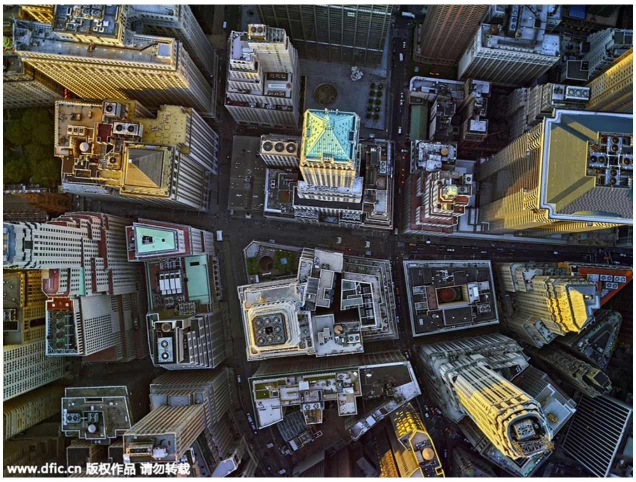

Figure 3.2: A bird's eye view of New York City [21].

an IA algorithm can take advantage from the prior information on where the UEs most frequently enter an area. To that purpose, ad-hoc algorithms, as the ones in [17], have to be conceived.

Figure 3.3: Example of a real street environment.

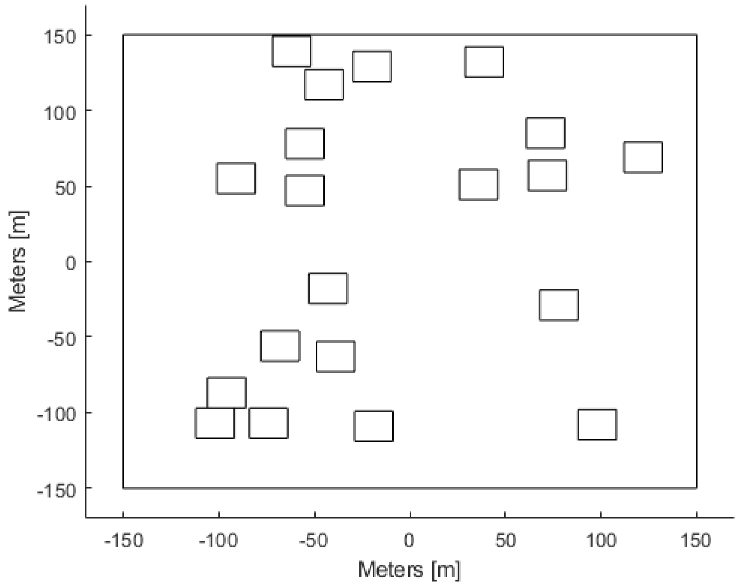

Figure 3.4: Example of *random* scenario with 20 obstacles.

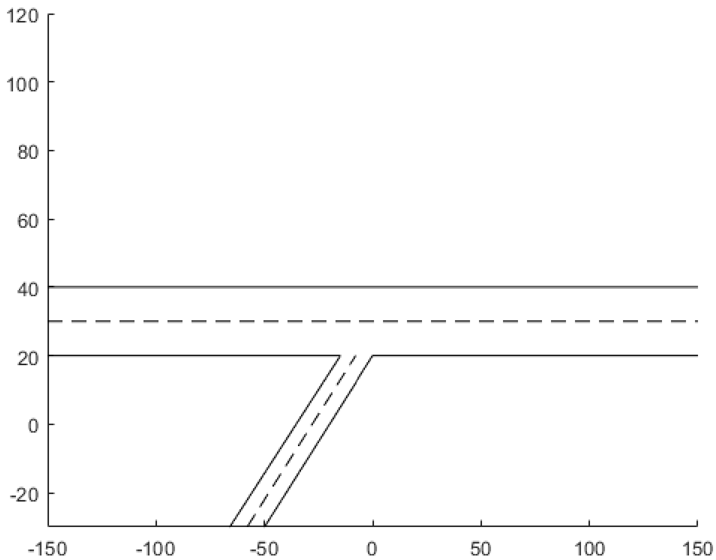

Figure 3.5: Example of street scenario with no obstacles.

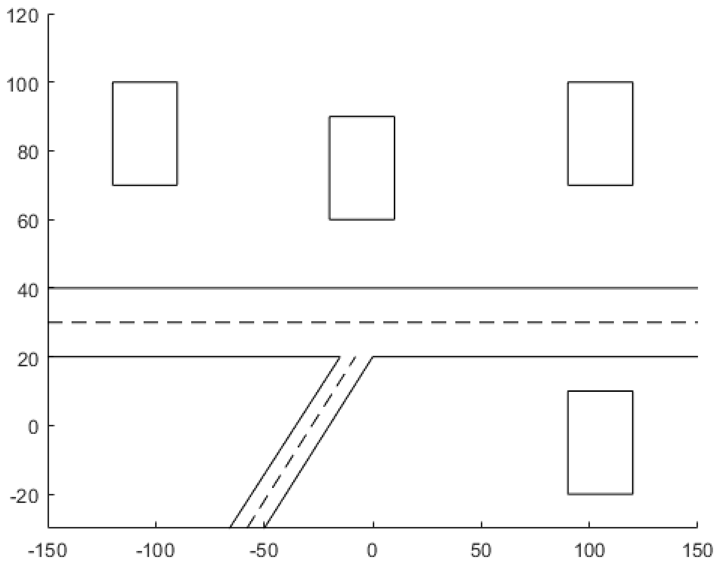

Figure 3.6: Example of street scenario with 4 obstacles.

3.2 BSs and UEs Generation

Once the scenario is determined, UEs and BS are placed in the environment according to their pre-determined number.

In the *random* scenario the BS is set in the centre of the area (case with only one BS), while the UEs are generated according to a *random* uniform distribution. Figure 3.7 shows the aforementioned environment, with one BS, 5 UEs and 10 obstacles inside the scenario. The aim of this type of generation is to simulate an environment where UEs appear suddenly inside the cell, like people coming out of houses. This concept leverages on the hypotheses that UEs inside a house are not reachable due to the blockage behaviour of mmWave propagation [4].

For this scenario we have also implemented a non uniform generation for the UEs. In this case the UEs are generated in three different areas with uniform probability inside.

Figure 3.8 shows an example of non uniform generation of the UEs. Unlike the previous UEs generation, Fig. 3.8 shows the presence of most of the UEs in three different spots, marked by the black, the green and the red rectangles. There are also two UEs, indicated with the black arrows, that appear outside the three crowded areas within the colored boxes. The generation mechanism is as follows: once a UE is generated it has 3 different probabilities, set a-

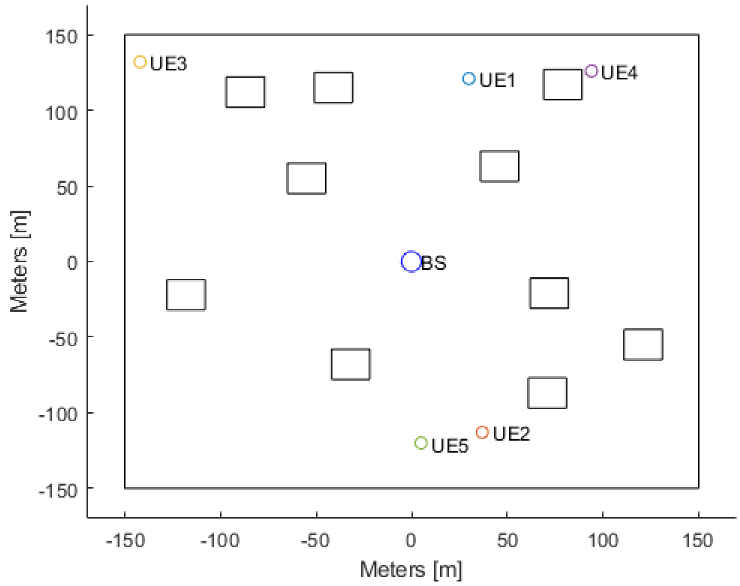

Figure 3.7: Example of *random* scenario with 10 obstacles, 1 BS and 5 UEs.

priori to being generated inside one of the rectangle. There is also a little probability for an UE to being generate outside the rectangle. Inside the rectangles the UEs are setted with a uniform probability. This generation is related to the same concept considered in the *fixed* geometry scenario, but in this case, thanks to the random location of the scatterers, this scenario reproduces a larger variety of real environments.

In the second scenario, as the one depicted in Fig. 3.9, the BS is positioned near the main street, while the UEs generation is bounded in three different locations. This particular generation is useful to simulate the street-like behaviour of the environment, for example in an hour of the day when is more likely for the car in the street to enter the cell from the right side instead of the left side. Figure 3.9 shows three different UE positions generated according to a uniform distribution inside the three possible areas, marked by the rectangles. As the previous generation, once a UE is generated it has three different probabilities to appear in the different areas of the street. Once the area is established, the position is determined according to a uniform distribution, since the user might not been detected immediately after its entrance in the cell.

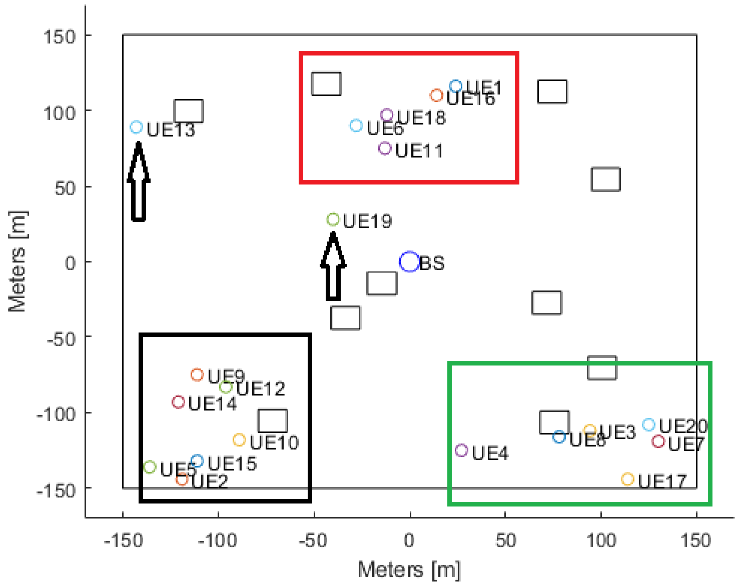

Figure 3.8: Example of non uniform generation in the *random* scenario.

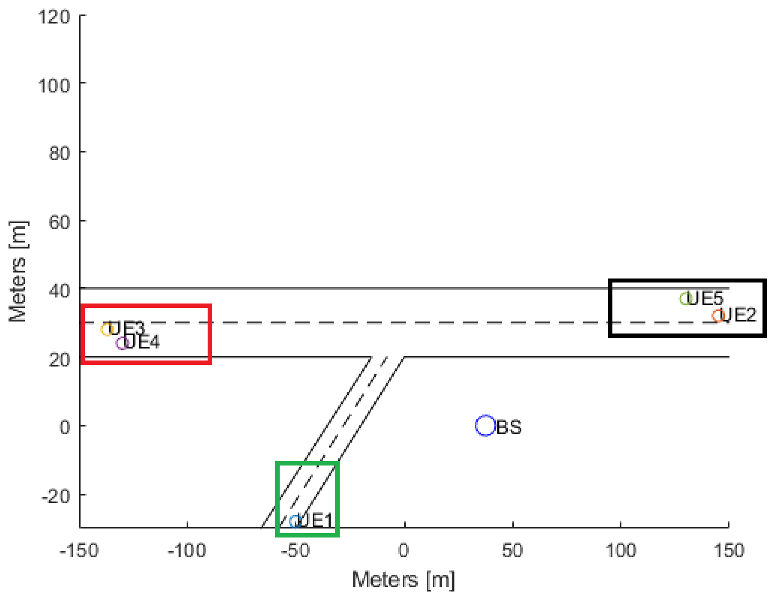

Figure 3.9: Example of *fixed* scenario with no obstacles, 1 BS and 5 UEs.

3.3 Channel Model

For the mmWave radio channel model we implemented a simple ray tracing software, realized in Matlab by following the guidelines in [13]. The main concept of our approach leverages on the high reflecting properties of walls at high frequency [22].

Thanks to the aforementioned information, our ray tracing function computes the direct path and the reflected paths (thanks to the principle of the images) from the BS to the considered UE. Only first order reflections are considered because of the experienced high path loss at mmWave whereas second order reflections are neglected.

The path loss model used in our work, i.e., a dual slope model designed with a 60 GHz carrier frequency, is the same as in [13] which is based on [12]. The formulas for the direct (PL) and the reflected path (PL_r) are defined as follows:

$$\mathrm{PL}(l) = 82.02 + k \cdot 10\ \log_{10}\left(\frac{l}{l_0}\right) + l \cdot \alpha_{O_2}; \tag{3.1}$$

$$\mathrm{PL}_R(l_r) = 82.02 + k \cdot 10\ \log_{10}\left(\frac{l_r}{l_0}\right) - R - F + l_r \cdot \alpha_{O_2} \tag{3.2}$$

where l and l_r depict the length of the LOS and NLOS path, respectively. l_0 represents the reference distance, here set to 5 m and the propagation factor k is 2.36, if the distance between the transmitter and the receiver is larger than the reference distance, or 2.00 otherwise. R and F include the reflection losses in the form:

$$R = 20\ \log_{10}\left(\frac{\sin\theta - \sqrt{B}}{\sin\theta + \sqrt{B}}\right),\ B = \epsilon - \cos^2\theta; \tag{3.3}$$

$$F = \frac{-80}{\ln 10}\left(\frac{\pi\sigma\sin\theta}{\lambda}\right)^2. \tag{3.4}$$

More specifically, R is the square of the Fresnel reflection coefficient in dB considering a TE polarization for the transmitted waves, defined as the ratio between the reflected and the incident fields.

In 3.3, 3.4 ϵ and σ represent the roughness and reflection coefficients of the material (namely, $\sigma = 0.2$ mm and $\epsilon = 4+0.2j$ [12]), while θ the reflection angle of the reflected path.

Finally, α_{O_2} represents the oxygen loss, which is non negligible at 60 Ghz. Figure 3.10 shows the values of the specific oxygen attenuation α_{O_2} in $[dB/Km]$

as a function of the frequency f and considering the following standard conditions for the atmosphere: pressure = 1013 hPa, temperature = 15 °C, humidity = 7.5 g/m^3. Notably, there is a peak in correspondence of $f = 60$ Ghz which correspond to a specific attenuation of 15 dB/Km.

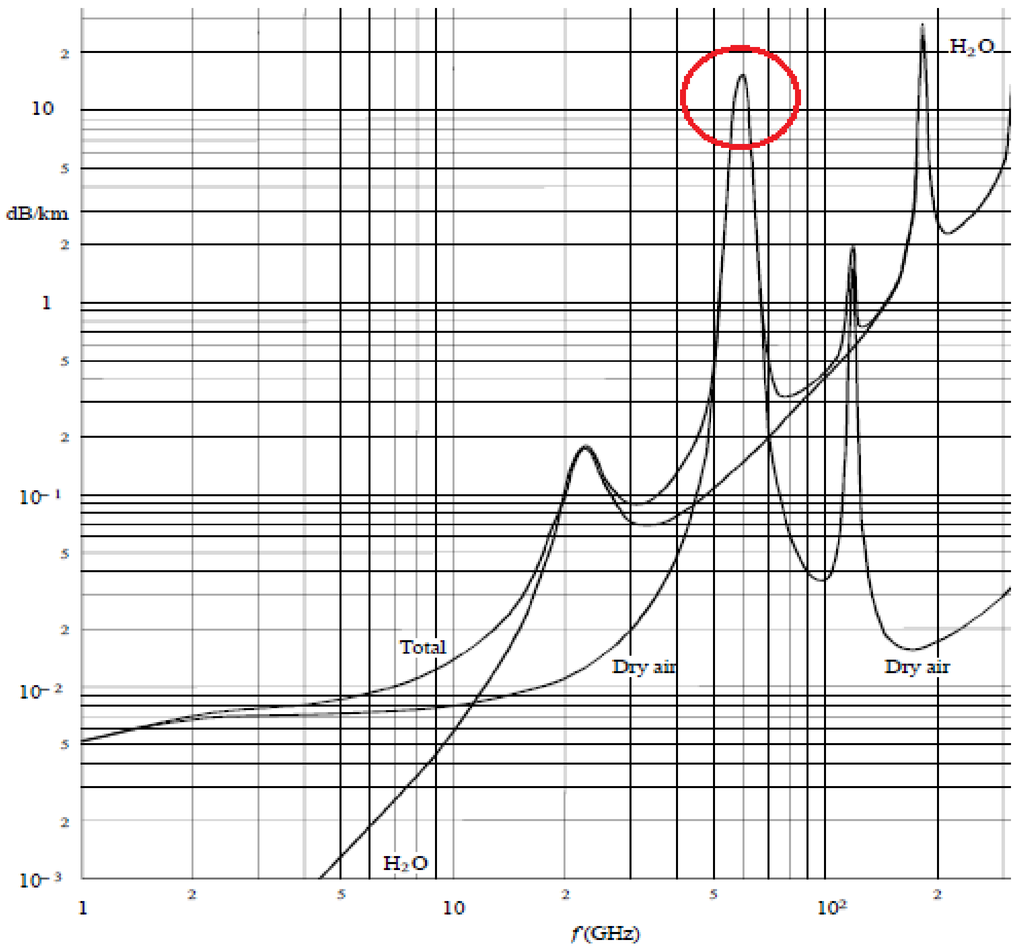

Figure 3.10: Oxygen specific attenuation for different frequencies. [23].

Figures 3.11 and 3.12 show some examples of channel realizations while using the model previously described. In particular, the dashed lines represent the direct rays, while the continuous lines represent the reflected rays. Considering Fig. 3.11, in this scenario only one UE (i.e., UE1 in the figure), is unreachable for the BS, since it has no direct path or first order reflections for connecting. The other UEs can instead establish a connection with the BS if and only if, the received power at UE side is greater than a certain threshold λ (described later). Fig. 3.12 shows an example of scenario where each UE-BS channel presents at least two paths.

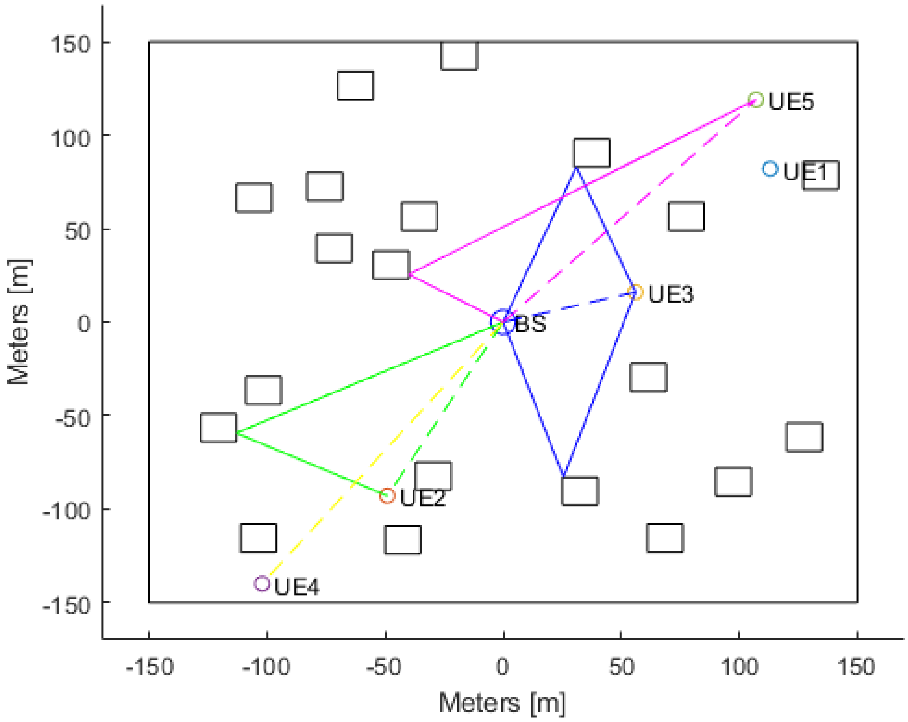

Figure 3.11: Example of channel realization in the *random* scenario with 20 obstacles, 1 BS and 5 UEs.

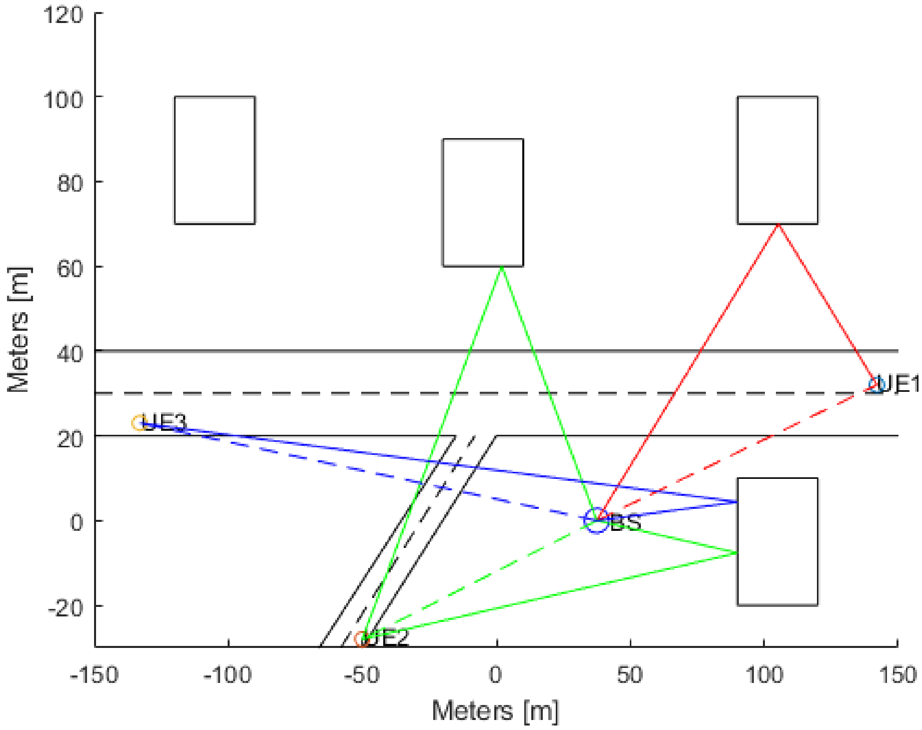

Figure 3.12: Example of channel realization in the *fixed* scenario with 4 obstacles, 1 BS and 3 UEs.

3.4 Antenna Models

In our work we have chosen the antenna model described in [12]. This model has been considered for its simplicity and because it takes into account the essential characteristics of the real world phased antenna array.

In particular, we define ϕ_{-3dB} and θ_{-3dB} as the HPBW in azimuth and elevation-planes, respectively, and ϕ_0 and θ_0 as the azimuth and tilt angles of the direction of the main lobe (Fig. 3.14). Fig. 3.13 in the right side shows the definition of the HPBW.

The expression of the array gain can be obtained starting from a two-dimensional Gaussian function, as in [12], used to express the main lobe gain in the form:

$$\mathrm{G}(\phi', \theta') = G_0 \cdot \exp(-\alpha\phi'^2) \cdot \exp(-\beta\theta'^2), \tag{3.5}$$

where ϕ' is the azimuth angle in the range $\{-\pi, \pi\}$, θ' is the elevation angle in the range $\{\frac{-\pi}{2}, \frac{\pi}{2}\}$, G_0 is the maximum gain corresponding to the direction ($\phi' = 0$, $\theta' = 0$). According to Fig. 3.13, the constants α and β are determined by considering ϕ_{-3dB} and θ_{-3dB} in the form:

$$\frac{G(\phi', \theta')}{G_0} = \exp\Big(-\alpha\Big(\frac{\phi_{-3dB}}{2}\Big)^2\Big) = \frac{1}{2}; \tag{3.6}$$

$$\frac{G(\phi', \theta')}{G_0} = \exp\Big(-\beta\Big(\frac{\theta_{-3dB}}{2}\Big)^2\Big) = \frac{1}{2}, \tag{3.7}$$

which gives:

$$\alpha = \frac{4ln(2)}{\phi^2_{-3dB}}, \ \beta = \frac{4ln(2)}{\theta^2_{-3dB}}. \tag{3.8}$$

By including 3.8 into 3.5, it is possible to obtain:

$$\mathrm{G_{dB}}(\phi', \theta') = G_{0,\mathrm{dB}} - 12 \cdot \left(\frac{\phi'}{\phi_{-3dB}}\right)^2 - 12 \cdot \left(\frac{\theta'}{\theta_{-3dB}}\right)^2; \tag{3.9}$$

$$10\log(e) \cdot 4\ln(2) \approx 12. \tag{3.10}$$

The main lobe beam widths ϕ_{ML} and θ_{ML} are defined by considering -20 dB with respect to the maximum gain value G_0. Using 3.9 one can obtain the relation between ϕ_{ML} and ϕ_{-3dB} for θ' =0 and between θ_{ML} and θ_{-3dB} for ϕ' =0 as follows:

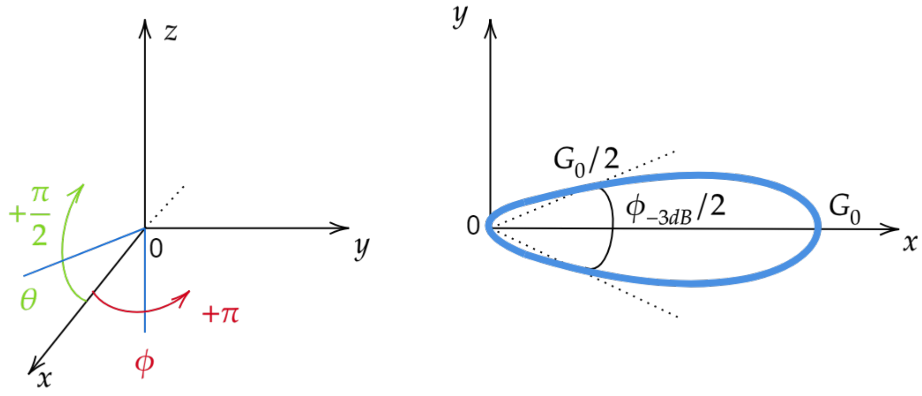

Figure 3.13: Coordinates system and half-power beamwidth definition.

$$\phi_{ML} \approx 2.6 \cdot \phi_{-3dB}, \quad \theta' = 0; \tag{3.11}$$

$$\theta_{ML} \approx 2.6 \cdot \theta_{-3dB}, \quad \phi' = 0. \tag{3.12}$$

The maximum gain G_0 can be written as:

$$G_0 = \frac{4\pi S}{\lambda^2}. \tag{3.13}$$

where S is the aperture size measured in square meters and λ is a wavelength.

Note that the beam width of the main lobe can be simply related to the rectangular antenna aperture physical dimensions using the following equations:

$$\phi_{ML} = \frac{2\lambda}{D_y}, \quad \theta_{ML} = \frac{2\lambda}{D_x}, \tag{3.14}$$

where D_x and D_y are dimensions of antenna aperture along x and y axes accordingly. Assuming that:

$$\text{S} = D_x \cdot D_y \tag{3.15}$$

it is straightforward to obtain:

$$G_{\mathrm{dB}}(\phi,\theta) = 10\log\left(\frac{16\pi}{6.76\cdot\theta_{-3dB}\phi_{-3dB}}\right) - 12\cdot\left(\frac{\phi-\phi_0}{\phi_{-3dB}}\right)^2 - 12\cdot\left(\frac{\theta-\theta_0}{\theta_{-3dB}}\right)^2. \tag{3.16}$$

Since we have only considered 2D environments, the third term is neglected so that the beam scans only the azimuth plane. Therefore, in the following we consider only the first and the second terms of the equation 3.16.

The second term of 3.16 allows to evaluate the gain as a function of the angles. In 3.16 the variables $\phi^{'}$ and $\theta^{'}$ have been substituted by $\phi - \phi_0$ and $\theta - \theta_0$ respectively. In particular, ϕ_0 indicates the beam direction in the azimuth plane, as shown in Fig. 3.14 (a). Fig. 3.14 (b) shows also θ_0 in the elevation plane, for the sake of completeness.

Note that ϕ_{-3dB} permits to define the number of *sectors* that the BS or the UE have to scan to cover the entire angular space. These sectors are listed into the *codebook*. The codebook is a table which contains the values of the gain for the entire angular space for each sector. For example a HPBW of 30° divides the space into 12 sectors.

The choice of the HPBW is fundamental for the IA algorithm: the larger is ϕ_{-3dB}, the lower is the number of sectors, hence a shorter time delay is needed to cover the whole angular space in search for UEs. On the higher side, the maximum gain is reduced, with a higher probability to wrongly miss a user detection.

An IA algorithm could leverage on multiple HPBW (i.e. more beam configuration) to reach a trade off between number of scans and misdetection probability, but with an increase in the complexity of the hardware. This aspect will be explored in the next chapter.

Fig. 3.15, 3.16 and 3.17 report three examples of beams used at the BS side, whereas Fig. 3.18 an example for the UE.

In addition, the aforementioned figures report also the beams for a different steering direction. More specifically, while the blue beam indicates the direction ϕ_0 =0°, the orange ones represent their counterpart for ϕ_0 =90°.

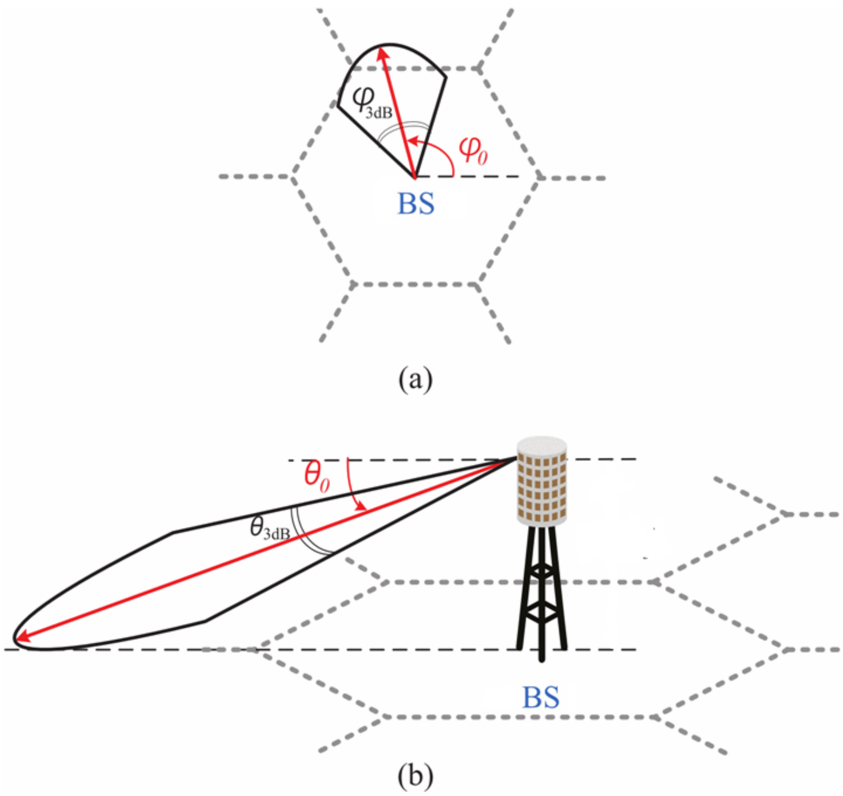

Figure 3.14: Example of the horizontal and the vertical beam patterns with the corresponding angles [20].

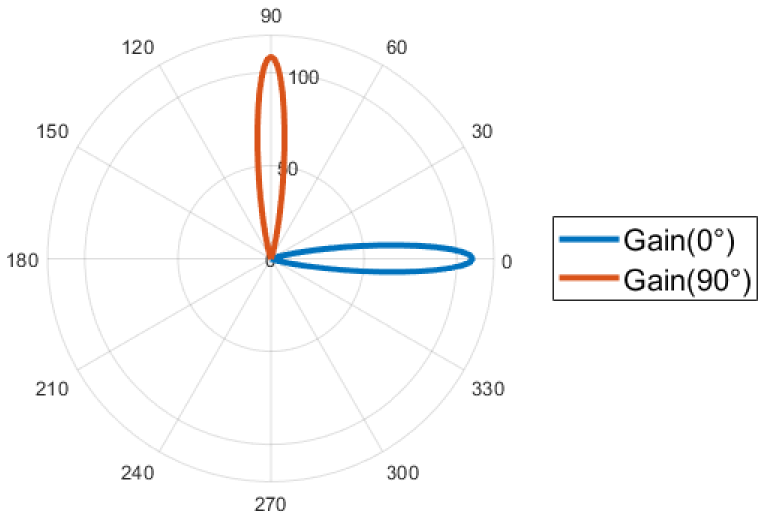

Figure 3.15: Base station radiation pattern with HPBW=15°.

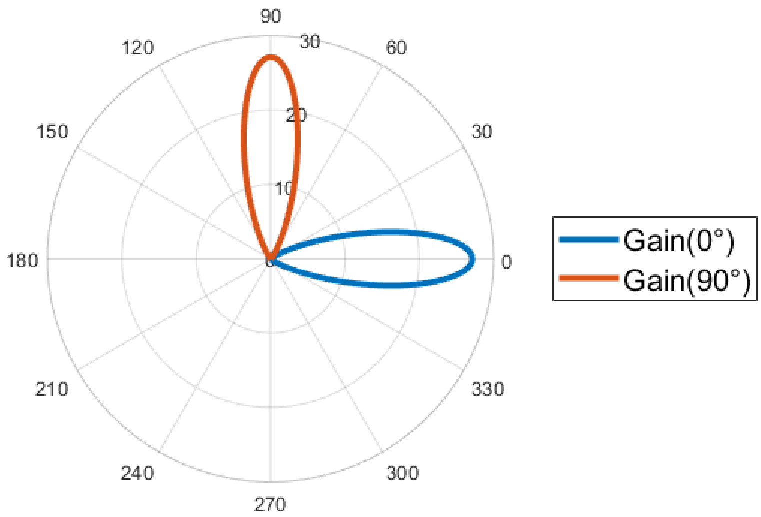

Figure 3.16: Base station radiation pattern with HPBW=30°.

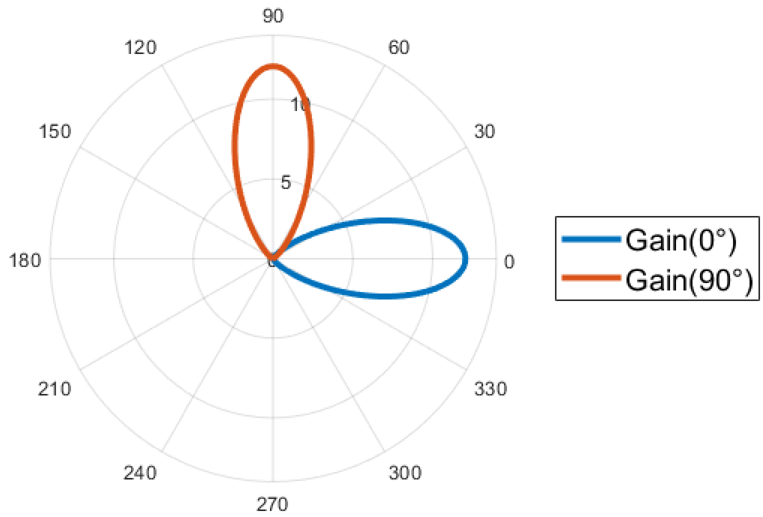

Figure 3.17: Base station radiation pattern with HPBW=45°.

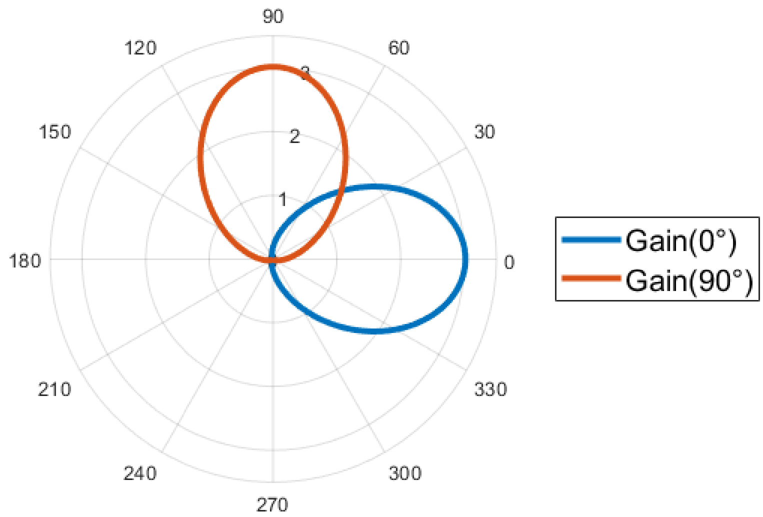

Figure 3.18: User equipment radiation pattern with HPBW=90°.

3.5 Implemented Algorithms

After having detailed the first three blocks reported in the flowchart of Fig. 3.19, we now describe how three algorithms inspired by the SOTA, as well as the proposed approaches of Sec. 2, are implemented in our simulator in Matlab.

For the sake of clarity, the description of the algorithms implementation is separated at BS and UE side.

3.5.1 Base Station Algorithms Implementation

We first show the three approaches inspired by the SOTA [13, 14, 16].
The flowchart 3.19 shows the common steps of the algorithms. First, during the initialization phase, the simulator sets the number of sectors at BS and UE side, that is, h and t, respectively. These numbers depend on the *codebook* dimension, and thus on the chosen HPBW. Moreover, the algorithm sets the value of the threshold λ (discussed in the last chapter), that represents the required power for UE detection.

After that, the algorithms work as follow:

- the BS steers its beam according to its *codebook*;
- for each beam of the BS there are two possibilities: if the UE is omni-directional the power budget is computed immediately. Otherwise the UE first steers one of its beam.
- for each combination BS-UE the received power P_r is compared with the threshold. If the UE is not found yet the algorithm returns to the step before, otherwise the process is stopped;
- if the UE has not been seen, the process stops and the UE is declared unreachable;
- if the UE leverages on beamforming the number of overall scans is augmented of a factor 4 (number of UE sectors).

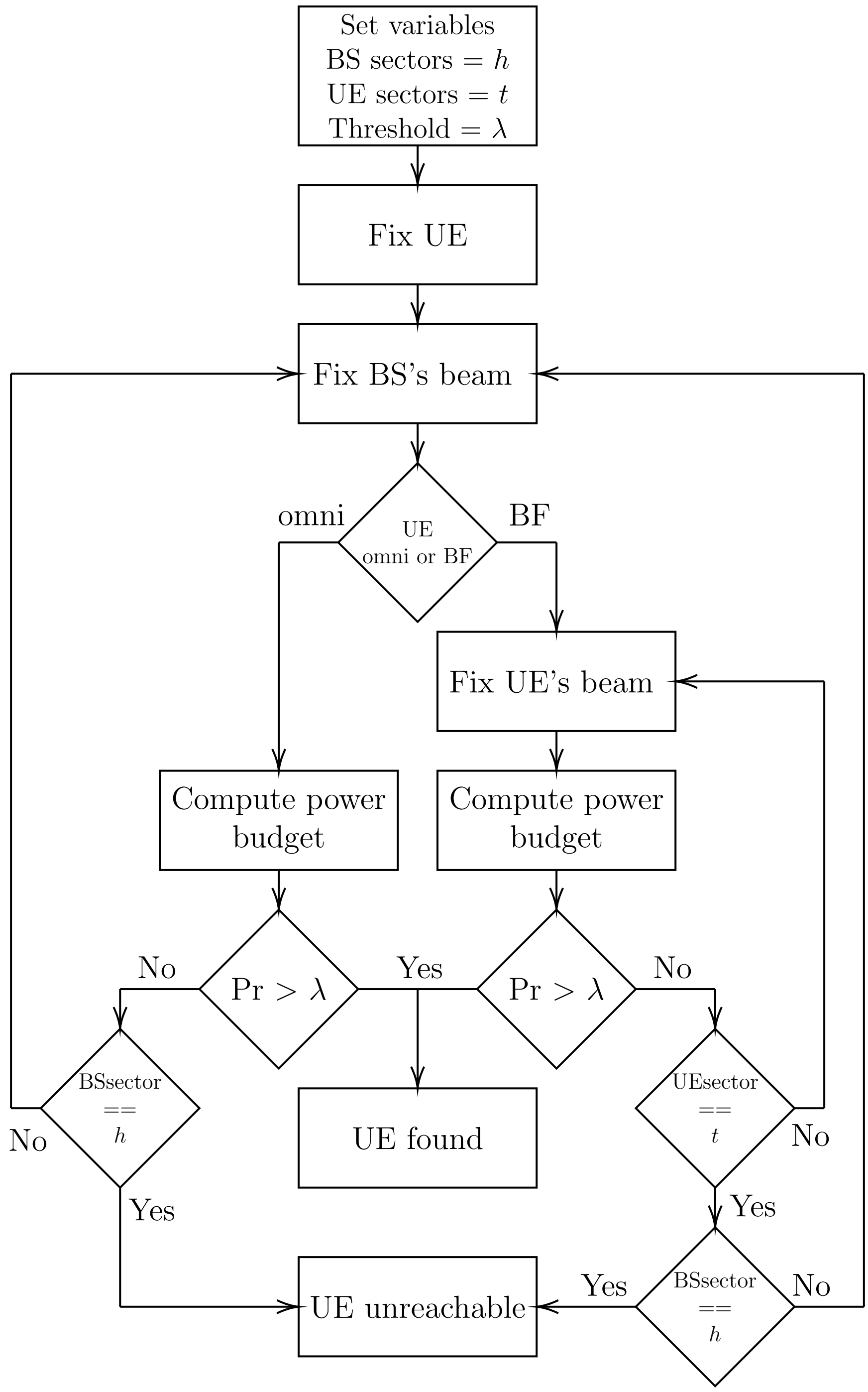

Figure 3.19: Flowchart which shows how algorithms in the simulator work.

Memory Less Search

The first considered approach is inspired by the EA in [14] where the area is scanned with a fixed HPBW from the first sector to the last one in a counter clock-wise manner.

The main difference between the algorithms is that, as explained in 1.3.1, the approach in [14] aims to find the best channel between the UE and the BS, whereas in our implemented memory less search (MLS) approach, the search stops as soon as the UE is detected, regardless it is whether or not the most suitable channel configuration.

The MLS is a simple SA algorithm, but it might cause a high discovery delay for the UE. This algorithm has been named MLS because the order in which the sector are steered is fixed, without the use of a memory, unlike the following algorithms.

Memory Based Search

With respect to the previous algorithm, this one leverages on the exploitation of a memory, that takes into account the number of historical users saw in every sector. This memory based search (MBS) follows the concept explained in [16], described in 1.3.2.

Notably, in this case there are few differences with the flowchart in Fig. 3.19: in the first step two vectors are defined, that is, $\mathbf{S}$ and $\mathbf{U}$. $\mathbf{S}$ is a vector which takes into account the sequence of sectors that the BS has to scan, while $\mathbf{U}$ is a vector of counters where each counter is associated to a sector, that is:

$$\mathbf{S} = [S_1..., S_j, ...S_k]; \tag{3.17}$$

$$\hat{\mathbf{S}} = [\hat{S}_1..., \hat{S}_j, ...\hat{S}_k]; \tag{3.18}$$

$$\mathbf{U} = [U_1..., U_j, ...U_k]; \tag{3.19}$$

$$\mathbf{I} = [I_1..., I_j, ...I_k]. \tag{3.20}$$

Figure 3.20 shows the added steps in the "UE find" block with respect to the MLS algorithm.

Initially, the element U_j is incremented by one, where S_j is the j th sector where the user has been found. Then, $\mathbf{U}$ is ordered in descent way, permitting to obtain the vector $\mathbf{I}$ which contains the indices of the sectors, from the one with the largest number of users, till the one with the lowest number. Finally the vector $\mathbf{S}$ is arranged using the indices in $\mathbf{I}$. The vector $\hat{\mathbf{S}}$ represents the new order of steering of the beams.

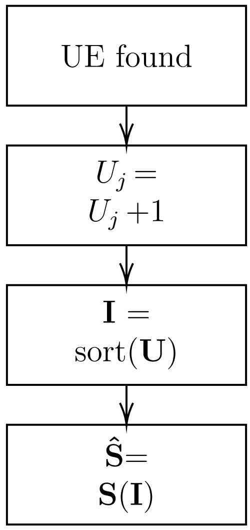

Figure 3.20: Flowchart of the memory-based fundamental part.

Database Search

This algorithm follows the idea considered in [13], explained in 1.3.6. Unlike the previous approaches, this is a NSA algorithm since it relies on a sub-6 GHz LTE control channel that provides, at the BS side, the knowledge of the GPS coordinates of the UEs once they enter the 5G cell. The main aspect of the algorithm is that the BS has a database like the one explained in 1.3.6, with the difference that in our case the width of the beam is fixed, so that the database contains only the information about the position of the previously detected users and the beam direction at BS side used to reach them.

When a user enters the cell, the GPS coordinates are transmitted to the BS with uncertainties σ_x and σ_y on the coordinate x and y, respectively. The BS computes the euclidean distance between every UE in the database and the selected UE. When a stored UE is considered close to the new one, that is the euclidean distance between the old UE and the new UE is less than a certain range m, the beam used to reach the old user is saved into a vector **D**.

Once the algorithm has controlled the whole database, the BS steers its beams starting from the directions saved in **D**. If the user is found the algorithm stops and the information on the UE detection is stored in the database. Otherwise if, after the scan of the whole database, there are no matches for a certain UE, or the UE has not been detected with the beam stored in **D**, the BS steers its beam starting from the directions which are closer to the GPS coordinates of the UE and then considering the further ones if the UE has not been detected. If the UE is found the BS saves the estimated position and the direction used in the database. If the UE is not detected it is considered unreachable.

Novel Search Algorithm

Here we provide the implementation details at BS side concerning our proposed algorithm described in 2.1. Considering the flowchart 3.19 this algorithm follows the main steps of it, but in the first step, a matrix is also initialized and used to memorize the found users.

First of all, we considered $H^{(N_{Beam})} = 15°$ and 3 values of the HPBW, thus our matrix has $N_{Sect} = 24$ columns and $N_{Beam} = 3$ rows. Fig.3.21 shows the considered HPBW from the wider to the thinner. Therefore, there are three elements in the vector **H** and **C**: Eq. 3.21 and 3.22 show the vector of the considered HPBWs and the corresponding configurations, respectively:

$$\mathbf{H} = [45°,30°,15°]; \tag{3.21}$$

$$\mathbf{C} = [C^{(1)}, C^{(2)}, C^{(3)}]. \tag{3.22}$$

Fig. 3.22 shows the correspondence between the HPBWs and the configurations in the table, while Fig. 3.23 shows an example of a matrix obtained in a simulation with 100 UEs dropped into the *random* scenario with the non uniform generation. The height of the bins corresponds to the number of UEs detected with the specific HPBW and steering direction of the beam.

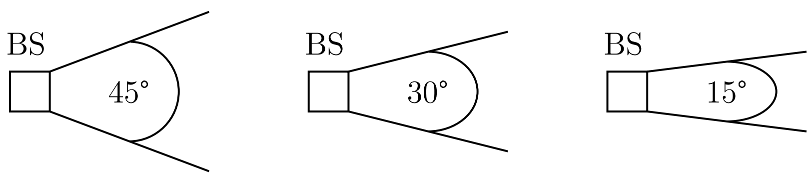

Figure 3.21: Beams widths at BS side.

With respect to Fig. 3.23, with 1 we indicate the configuration on the table corresponding to the larger beam (HPBW = 45°), because a UE detected with this beam width is a user near to the BS, i.e. with a high received power. Therefore, since such beam is three times wider than the thinner beam, it has to occupy three cells in the matrix, so one sector of this beam corresponds to three sectors of the thinner beam. The indicator 2 indicates instead the configuration on the table correspondent to the second beam width (HPBW = 30°). A UE detected with such beam might correspond to a low power level UE, because the second beam width could detect even the low power level UE as the third beam width, or a mid power level UE which can not be detected by the largest beam. Since the second beam width is two times the thinner one, it corresponds to two columns. Finally, the indicator 3 indicates the configuration for the first beam width. This beam permits to detect every possible user in a column with a received power more higher than the threshold.

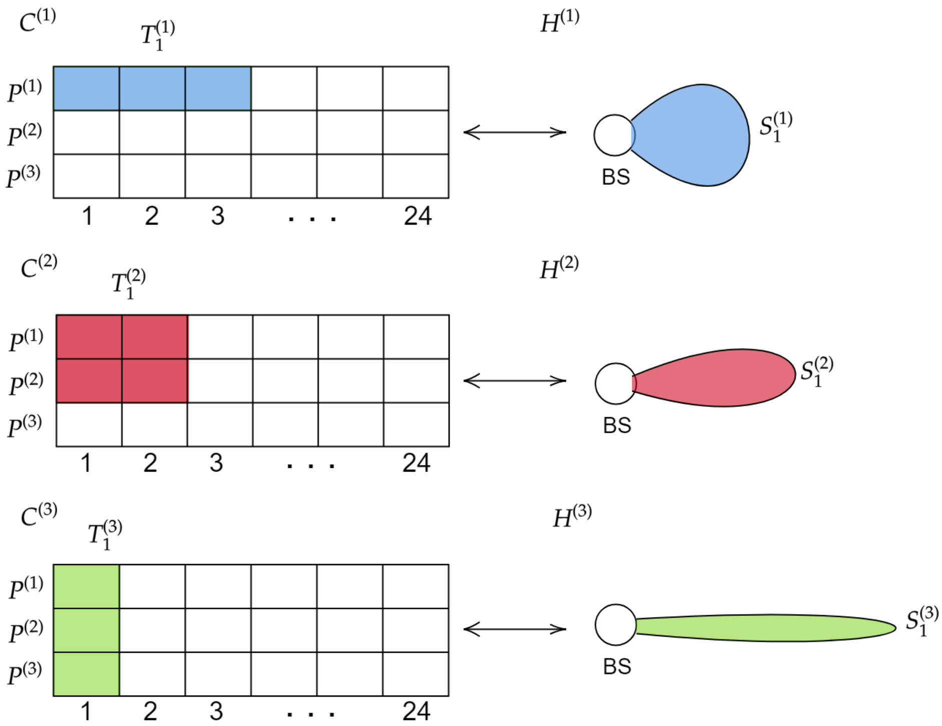

Figure 3.22: Scheme which shows the equivalences between the configurations in the table and the HPBWs of the correspondent beams widths.

The results obtained with this algorithm are discussed in the last chapter.

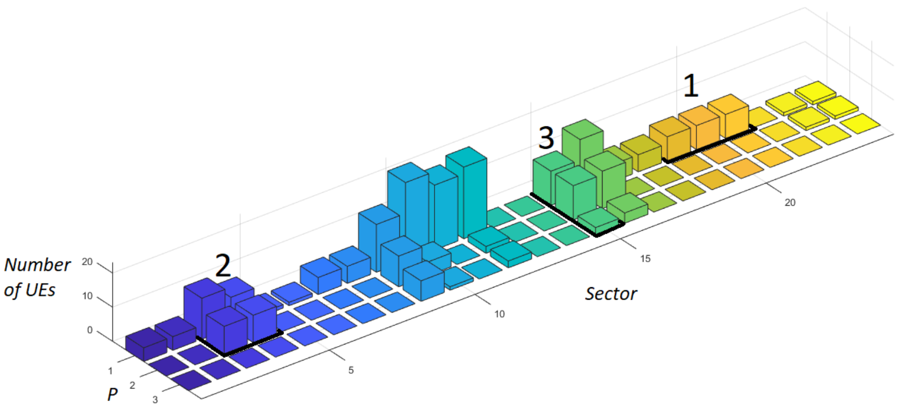

Figure 3.23: Example of BS table. The three indicator 1, 2 and 3 show the three type of configurations considered in our implementation of the algorithm.

3.5.2 User Equipment Algorithms Implementation

In this section we provide a description of the algorithms for the UE side that we have implemented in Matlab. Since an omnidirectional antenna can not modify its steering directions, we account only for the cases when the UE is equipped with an antenna array.

Memory Less UE Search

Like the MLS for the BS described in 3.5.1, once the BS has steered its beam towards a direction, the UE iteratively points its beam towards four predetermined directions, according to its *codebook*. Notably, such directions are a-priori setted, and the procedure stops once the UE has been detected. Fig. 3.24 shows the four direction of steering:

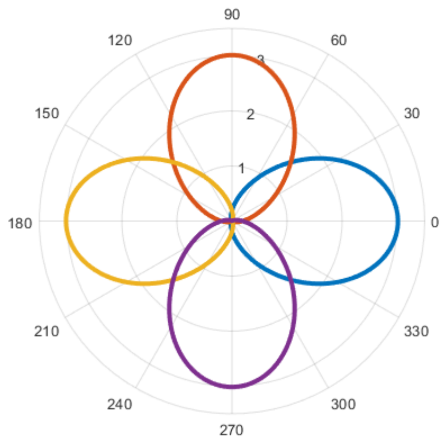

Figure 3.24: Beam steering in four a-priori decided directions.

Memory Based UE Search

Following the idea explained in Sec. 2.2 we implemented an approach smarter than the previous one in order to reduce the number of steering directions at UE side.

In our implementation of the algorithm the *database* is a matrix with a number of rows equal to the number of past UEs. The columns instead are three: the first two contain the x and the y coordinates of the i th UE, while the third column contains the sector in which the i th UE detected the BS.

The flowchart 3.25 shows the main steps of the algorithm.

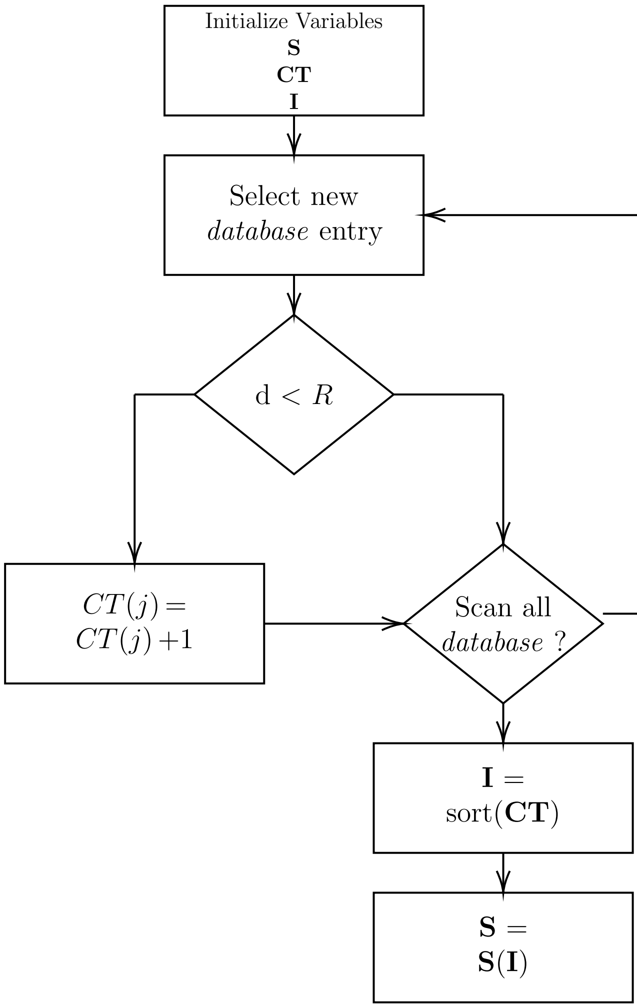

Figure 3.25: Flowchart of the smart UE approach.

Initially we defined three vectors: **S**, **CT** and **I**. The vector **S** contains the sequence of steering directions for the UE beams. In the beginning a default order is considered. **CT** instead contains the counters corresponding to the sector in **S**. Initially is a vector of zeros. Finally **I** is a vector of indices corresponding to the sectors in **S**.

When one UE enters the cell it computes the euclidean distance between its coordinates and the coordinates of each UE in the *database*. Whenever the new user finds a past UE which has detected the BS in a position within the range R, it increments the counter in **CT** associated to the j th sector in which the past user found the BS.

Once the UE has scanned the whole *database*, the elements of **CT** are put in descent order. The resulting indices in **I** are used to rearrange the vector **S**, which represents now the new order of steering directions.

Chapter 4

Numerical Results

This chapter reports the results obtained with the simulator implemented in Matlab. The experiments have been conducted using the Monte Carlo method. The table 4.1 shows the main parameters which we used for the numerical evaluations if not otherwise indicated.
More specifically:

- A carrier frequency of 60 GHz has been chosen, in accordance with the path loss model described in Chapter 3;
- The transmitted power are set to $P = 1\,\mathrm{W}$, in accordance with [13,14];
- The power threshold has been chosen according to [13];
- The HPBW at UE side has been considered in conformity with [14], while the HPBWs at BS side according to [13].

We considered two types of simulations for the two different scenarios. The simulations for the *random* scenario are implemented considering three Monte Carlo cycles:

- An external cycle where, for each iteration, the size of the cell is set;
- An intermediate cycle, where the position of the obstacles in the scenario is determined;
- The last inner cycle, where UEs are generated, and the IA algorithms launched.

This type of simulation is useful to average the effect of the obstacles which are generated with a uniform distribution in the area. For this scenario the dimension of the cell has been varied from 20 meters to 150 meters.

Carrier Frequency	$f_c = 60\,\text{GHz}$
Transmitted power	$P_t = 0\,\text{dBW}$
Received power threshold	$\lambda = -103\,\text{dBW}$
HPBW at BS side	$\phi^{BS}_{-3dB} = 15/30/45\,°$
Maximum BS antenna gain	$G^{BS}_0 = 20.4/14.3/10.8\,\text{dBi}$
HPBW at UE side	$\phi^{UE}_{-3dB} = 90°$
Maximum UE antenna gain	$G^{UE}_0 = 4.79\,\text{dBi}$

Table 4.1: Parameters for numerical evaluation.

The simulation for the *fixed* scenario includes, instead, only a Monte Carlo cycle, in which we varied the dimension of the cell. For each cell size, the UEs are deployed into the scenario whereas the obstacles positions are fixed. We tested the *fixed* scenario with 4 obstacles. The dimension of the cell has been varied from 80 meters to 150 meters.

4.1 Evaluation of the Received Power

In this section we provide some examples of received power (P_r in [dBW]) at UE side with respect to the threshold λ. Figure 4.1 and 4.3 show the scenarios in which the simulation has been conducted, while Fig. 4.2 and 4.4 show the respective evaluated power at UE side. In particular, in the x-axis we reported the index of the sector at BS side, whereas in the y-axis the highest collected power for that index. The best steering direction for the UE is written with a text-arrow for each point. Notably, according to Fig. 4.2, the best configuration is achieved when the UE steers its beam towards its sector 3, whereas the BS towards its sector 2. Despite the small size of the cell, the received power is only a few dBs higher than the threshold, due to the experienced high PL.

Focusing on 4.4, since the UE in Fig. 4.3 is closer to the BS than in Fig. 4.1, the received power is higher. Indeed, the BS almost detects the UE when this steers its beam in the first sector. This because there is a reflected ray which has sufficient power to reach the threshold.

In both the scenarios, the UEs are detected thanks to the direct ray. This behaviour is due to the high losses for the reflected rays, which are always weaker than the LOS component.

To better corroborate the aforementioned considerations Fig. 4.5 shows the mean value of the PL for both the directed and reflected rays, as a function of the cell dimension. These curves are obtained using a Monte Carlo simulation in the *random* scenario. For each cell size, 10000 UEs have been randomly placed in the scenario in order to obtain the mean PL for both the direct and the reflected ray.

The PL for the reflected rays is always at least 15 dB greater than the PL for the related LOS paths. Hence, it becomes difficult to take advantage from the multipath when the LOS between the UE and the BS is not present. In fact, by accounting for the parameters herein considered, UEs in NLOS propagation conditions are usually not detected (misdetection event). Thus, in order to recover lost UEs it would be beneficial to increase the transmitted power level, that in real situations is always constrained by the power transmission mask.

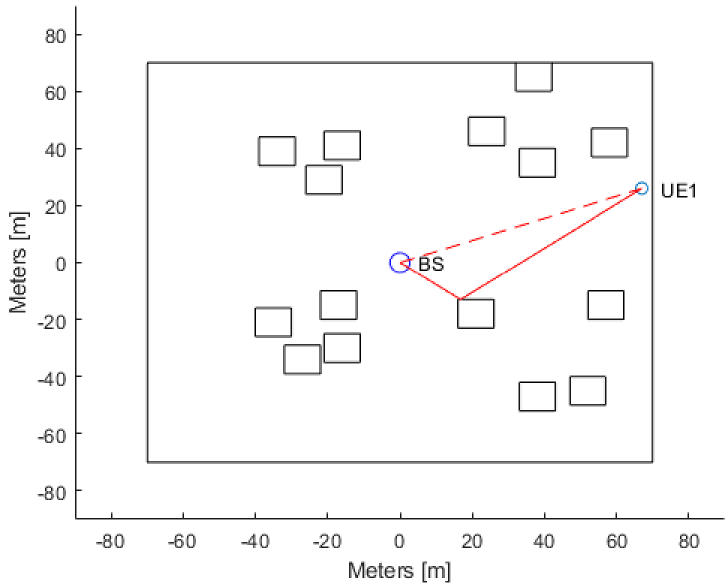

Figure 4.1: Generation of 1 UE in the *random* scenario.

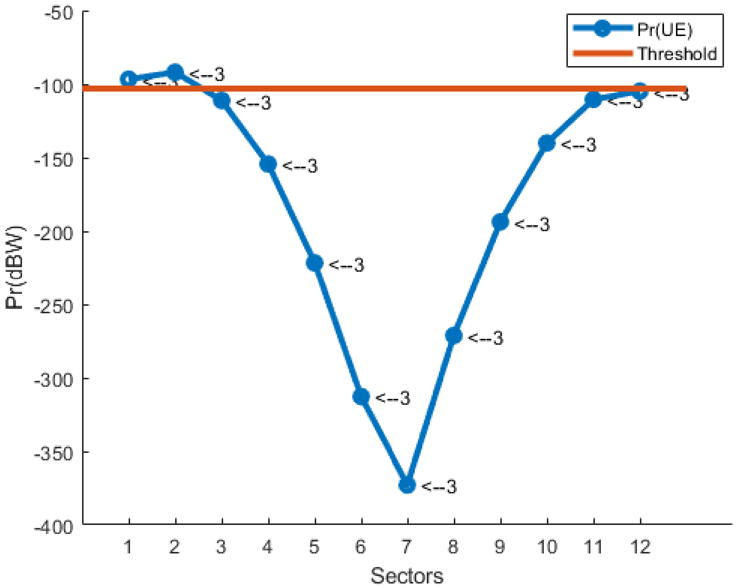

Figure 4.2: Received power at UE side, in the *random* scenario, for the different sectors at the BS side.

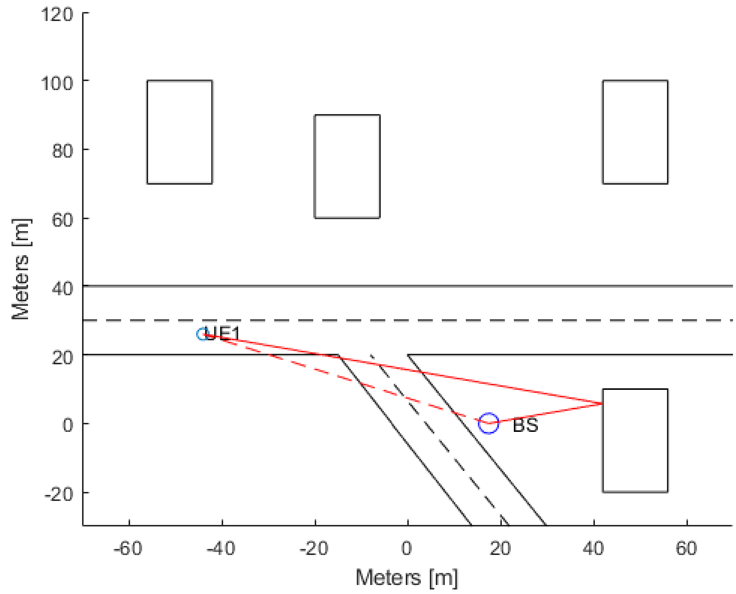

Figure 4.3: Generation of 1 UE in the *fixed* scenario.

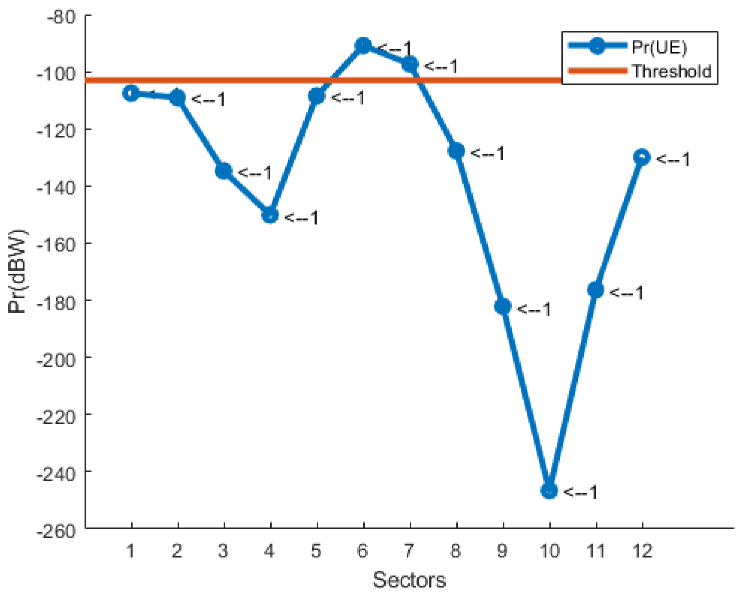

Figure 4.4: Received power at UE side, in the *fixed* scenario, as a function of the sectors at BS side.

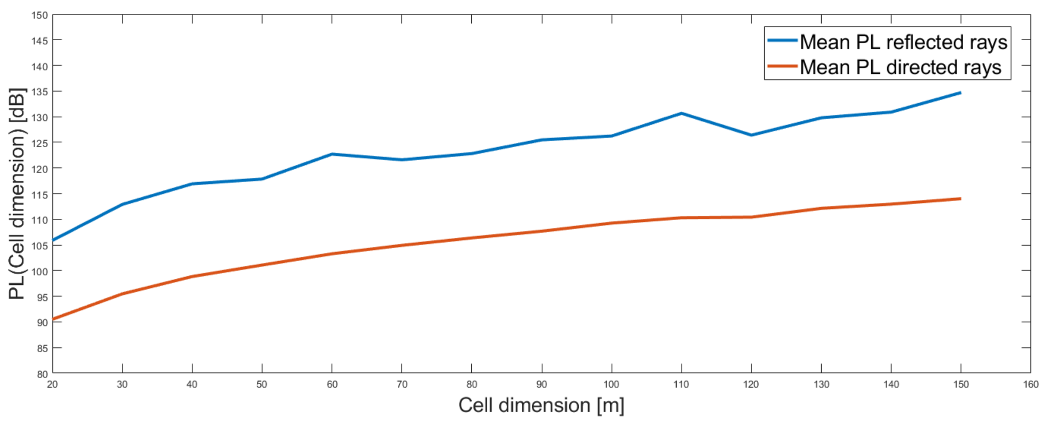

Figure 4.5: Path loss in dB as a function of the cell size for both the directed and the reflected paths.

4.2 Figures of Merit

The main target of the IA phase is that it has to be fast. In simple terms, the UE once it entered in a cell, has to detect a PSS from the BS immediately. Therefore, one of the most important figure of merit we have considered is the *average discovery time* evaluates in average number of scans required to establish a communication channel between UE and BS. In our simulations this figure of merits has been obtained through the sum between the scans at BS side and UE side.

Considering a scenario where the UE might be present (H_1) or not (H_0), the second figure of merit is related to the misdetection probability, defined as follows:

$$P_{MD} = P(\hat{H}_0|H_1). \tag{4.1}$$

where, $\hat{H}_0$ is the decision that the UE is not present. Thus, we defined the misdetection rate, as the ratio between the number of the misdetected UEs N_{MD} and the total number of UE generated in the scenario N_{tot} i.e.:

$$MD_r = \frac{N_{MD}}{N_{tot}}. \tag{4.2}$$

4.3 Memory Impact on the Performance

We now discuss the results obtained for the MLS and MBS algorithms described in Sec. 3.5, in order to evaluate the impact of the memory in the *random* and in the *fixed* scenario. We initially considered the UE generation, with a uniform distribution, in the *random* scenario. In these first simulations the BS HPBW is set to 30°. Figures 4.6, 4.7, 4.8, 4.9, 4.10 and 4.11 report the simulation results.

In particular, such results put in evidence how the memory considerably reduces the *average discovery time* with respect to the memoryless case. This happens for both UEs equipped with omni-directional or beamforming antennas. Focusing on Fig.4.6 and Fig.4.7 it is clear that the memory is useful not only for the *fixed* scenario, where the generation is non uniform, but also for the *random* scenario with uniform generation. This effect can ascribed to the fact that the memory somehow takes into account the positions of the obstacles. Hence, the sectors "shadowed" by obstacles are explored at last, because of the lower probability to detect UEs.

Obviously, the usage of the memory is more relevant in the *fixed* scenario, where the UEs are concentrated in specific positions.

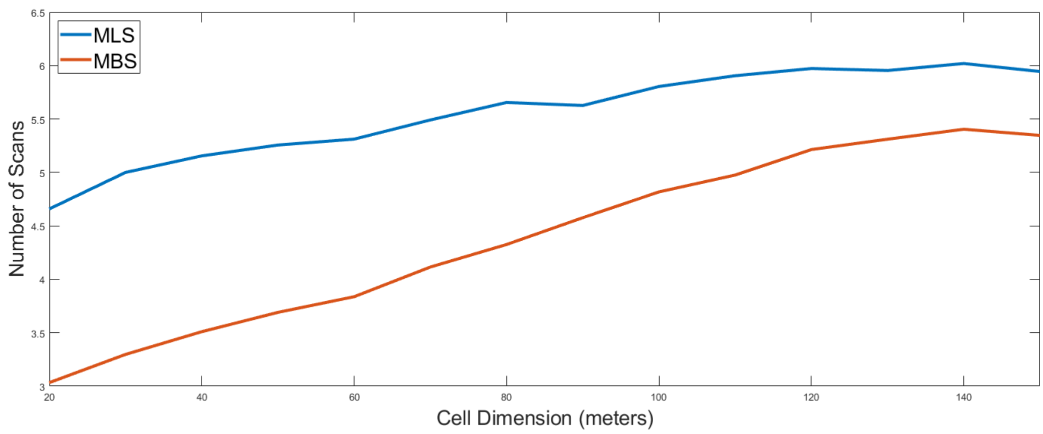

Figure 4.6: Mean number of scans vs cell dimension in the *random* scenario with uniform generation of UEs equipped with omni-directional antennas.

Concerning the performance in terms of misdetection ratio, reported in Fig. 4.8 and 4.11, the possibility to perform beamsteering at the UE side allows to improve the results with respect to the adoption of an omni-directional antenna. In addition, according to Fig. 4.8 the distance between the two curves is not very significant before 100 m because the misdtections are mostly due to the obstacles. When the distance becomes higher than 100 m the beamforming technique permits to reduce the misdetection, even if the gain at UE side is not very high. Furthermore, differences in the misdetection ratios are higher in Fig. 4.11 with respect to Fig. 4.8 due to how UEs are placed in the environment: in the *fixed* scenario the UE are always generated in the edge of the cell. Thus, it represents a worst case scenario in terms of path loss, but the BS and the UEs are always in LOS. On the contrary, in the *random* environment, even if the cell has the maximum dimension, the UEs could be generated close to the BS, because of the uniform distribution but the LOS condition is not always guaranteed.

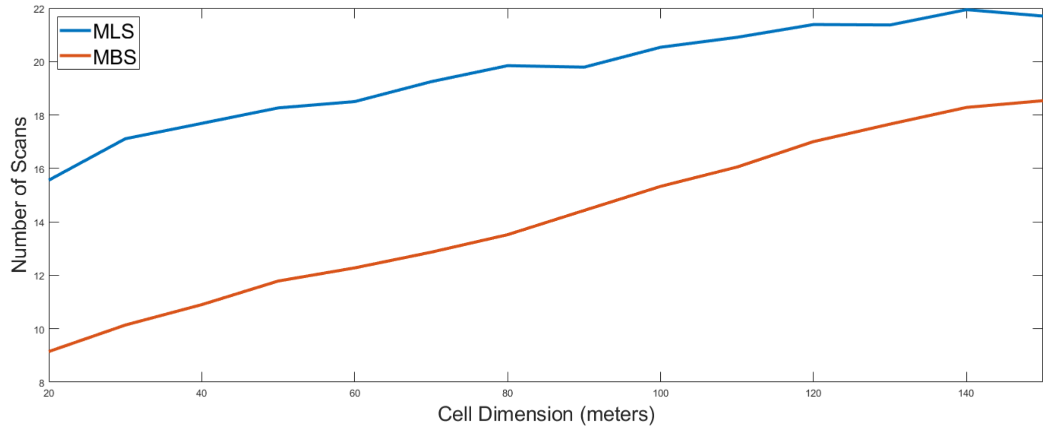

Figure 4.7: Mean number of scans vs cell dimension in the *random* scenario with uniform generation of UEs equipped with beamforming antennas.

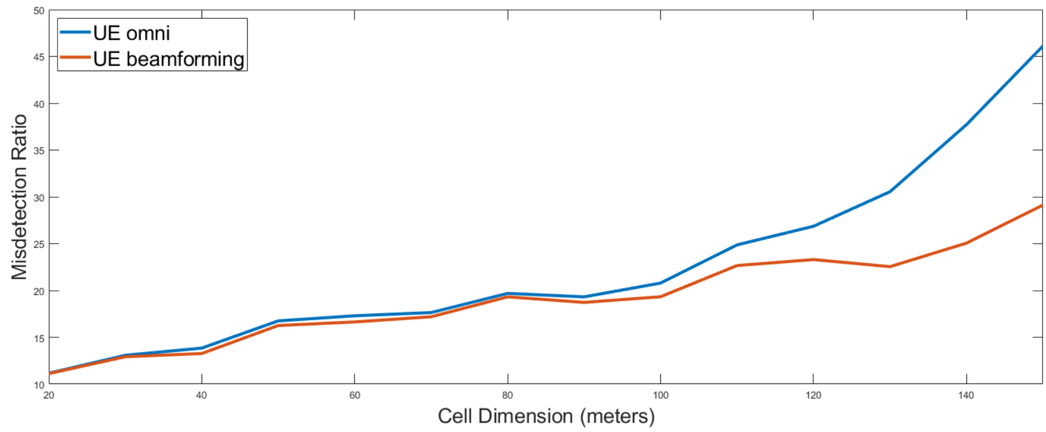

Figure 4.8: Misdetection ratio vs cell dimension in the *random* scenario with UEs equipped with beamforming antennas vs UEs equipped with omnidirectional antennas. This curve has been obtained with the MLS approach with HPBW = 30°.

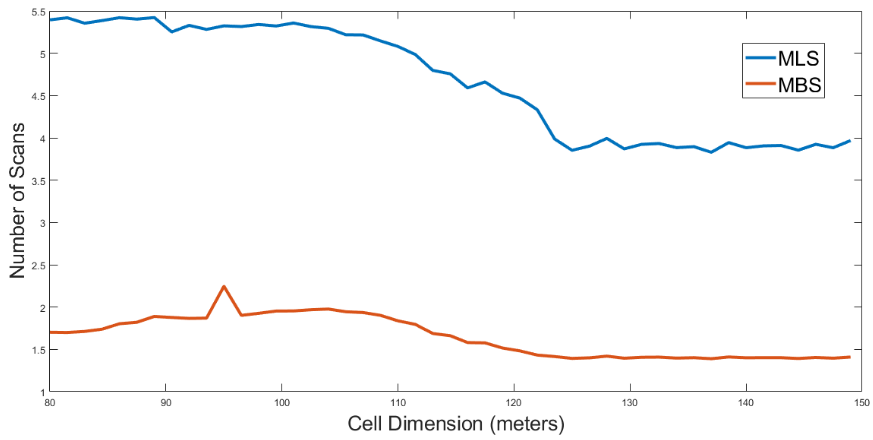

Figure 4.9: Mean number of scans vs cell dimension in the *fixed* scenario with non-uniform generation of UEs equipped with omni-directional antennas.

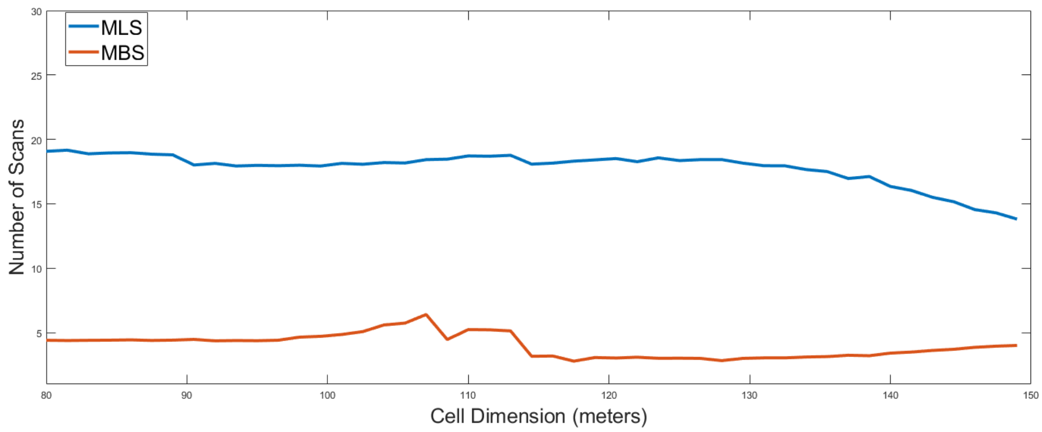

Figure 4.10: Mean number of scans vs cell dimension in the *fixed* scenario with non-uniform generation of UEs equipped with beamforming antennas.

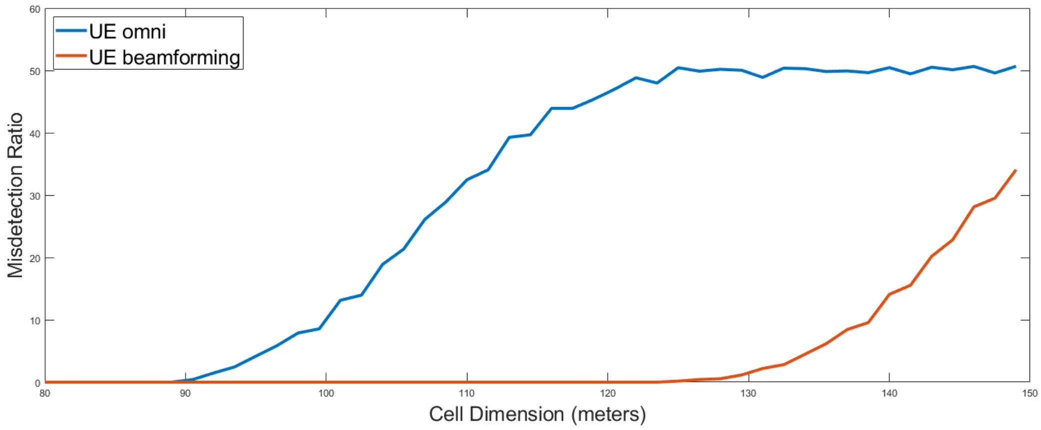

Figure 4.11: Misdetection ratio vs cell dimension in the *fixed* scenario with UEs equipped with beamforming antennas vs UEs equipped with omnidirectional antennas. This curve has been obtained with the MLS approach with a HPBW = 30°.

Since, the initially considered *fixed* scenario has been useful to appreciate the impact of the memory when a specific geometry is considered but, since it is not a representative environment, we included also the non-uniform generation for the *random* scenario. This allows to reproduce several and different *fixed* scenarios, in order to average the performance. Indeed, this generation of the UEs is more interesting than the previous one, because it is more representative of the real world, including different environments which are randomly created.

In this sense, Fig. 4.12, 4.13 and 4.14 show the performance obtained with the MLS and the MBS algorithm in these new conditions. Considering the comparison between the non uniform generation in the *random* scenario and the *fixed* scenario we noticed that results are very similar, as expected. Thus, in the following we consider only *random* scenarios that alternatively accounts for the uniform and non-uniform UEs generation.

The misdetecion ratio in Fig.4.14 shows worse performance than Fig. 4.8 since, when UEs are generated with a non-uniform distribution, they are more often placed in the edge of the cell.

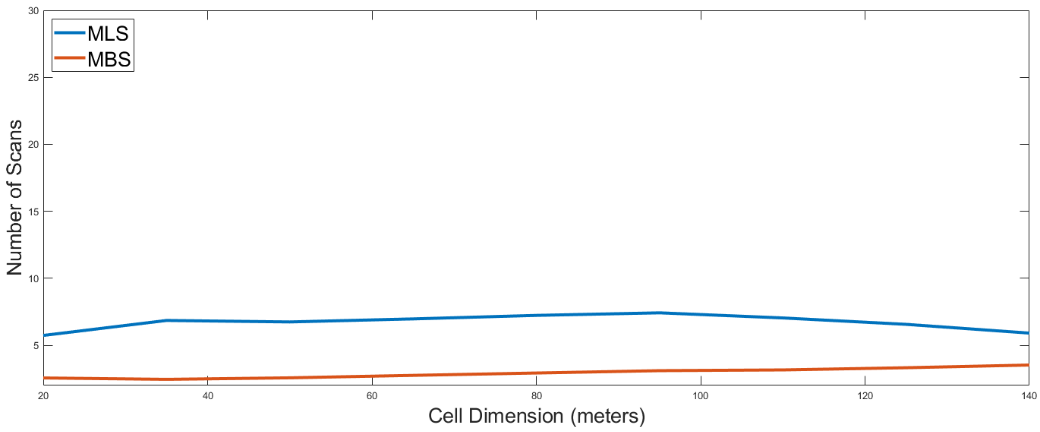

Figure 4.12: Mean number of scans vs cell dimension in the *random* scenario with non-uniform generation of UEs equipped with omni-directional antennas.

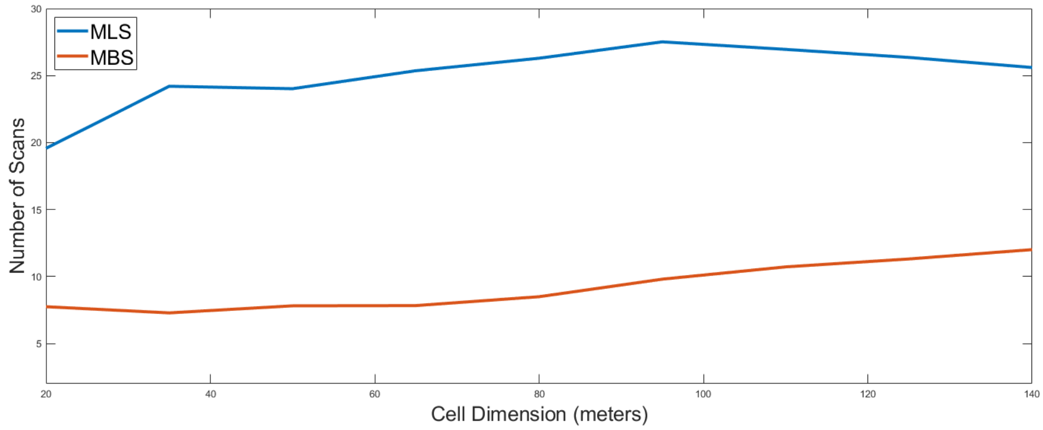

Figure 4.13: Mean number of scans vs cell dimension in the *random* scenario with non-uniform generation of UEs equipped with beamforming antennas.

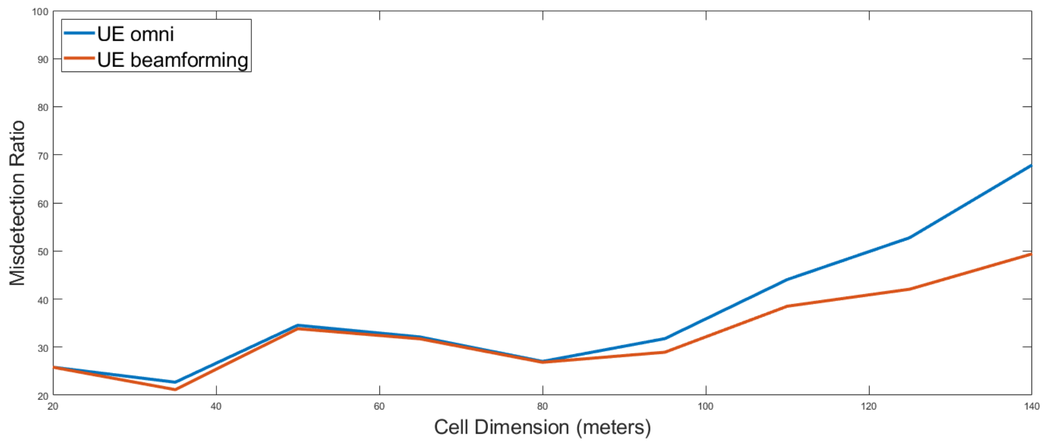

Figure 4.14: Misdetection ratio vs cell dimension in the *random* scenario with UEs equipped with beamforming antennas vs UEs equipped with omni-directional antennas. This curve has been obtained with the MLS approach with a HPBW = 30° and a non-uniform generation of the UEs.

4.4 NSA Algorithm Performance Evaluation

In the previous section we have evaluated the advantages obtained with a memory-based system. For example, Fig. 4.13 shows that for a SA approach taking into account the past UEs is fundamental to achieve a lower number of scans. Therefore, in order to evaluate how the memory together with the GPS coordinates can speed up the IA phase we also tested the NSA algorithm, explained in 3.5.1. We tested the algorithm with the 3 Monte Carlo nested cycle simulation, like the aforementioned. We fixed the GPS accuracy to $\sigma_{GPS} = 2\,\mathrm{m}$ following the consideration in [24].

Fig. 4.15 and 4.16 show that, leverage on a database based on the GPS coordinates lead to a great decrease in the IA phase with respect to the SA approaches shown before. Nevertheless, a dedicated control channel is required, hence with waste in spectral resources. These results motivated the design of a novel scheme aimed at improving the performance.

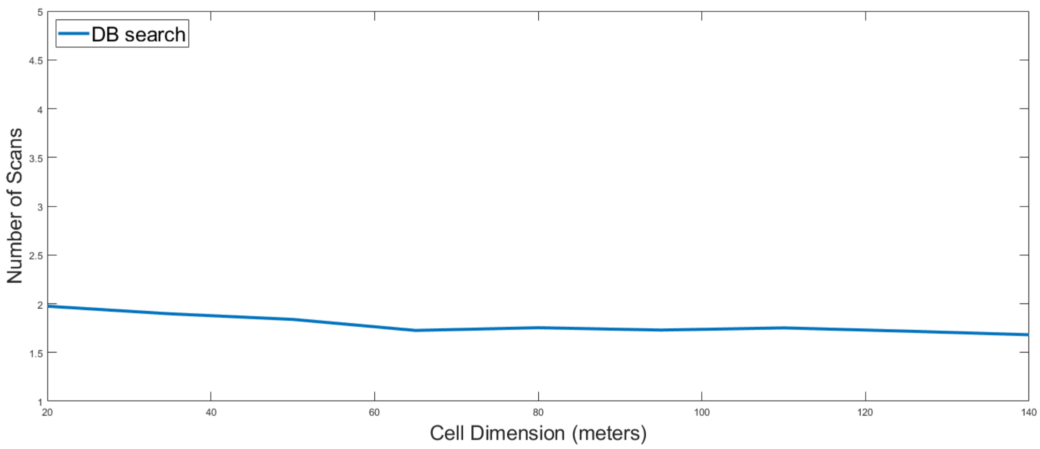

Figure 4.15: Mean number of scans vs cell dimension in the *random* scenario with uniform generation of UEs equipped with omni-directional antennas.

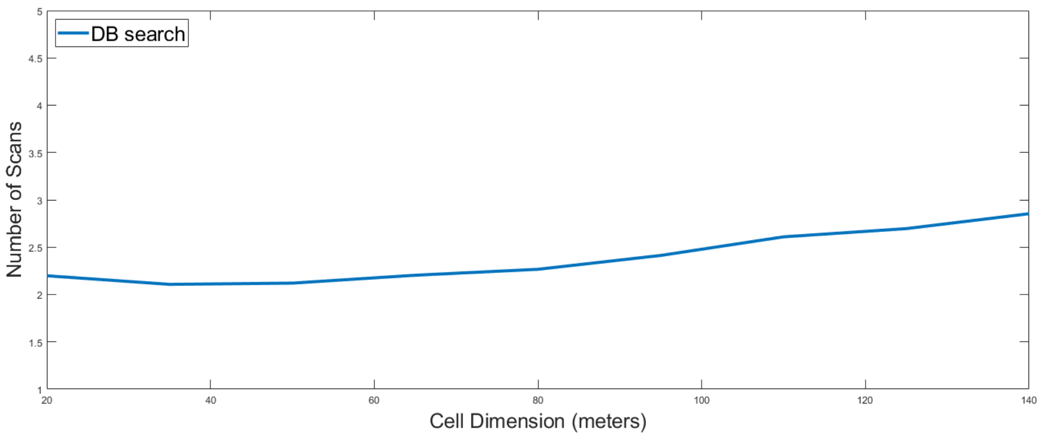

Figure 4.16: Mean number of scans vs cell dimension in the *random* scenario with uniform generation of UEs equipped with beamforming antennas.

4.5 Novel Approach Performance

In this section we finally compare the proposed approach, described in Chapter 2, with respect to the MLS and the MBS approaches, whose performance has been analysed in Sec. 4.3. More specifically, the proposed approach is first tested when the UE is considered equipped with an omni-directional antenna or with the memoryless beamforming technique, while successively when the UE has the capability to exploit a *database* containing prior information deriving from other UEs. In this simulations, in order to test each algorithm with the same misdetection ratio, we fixed the HPBW to 15° for the MLS and the MBS algorithm. We test the algorithms in *random* scenario with both uniform and non uniform generation.

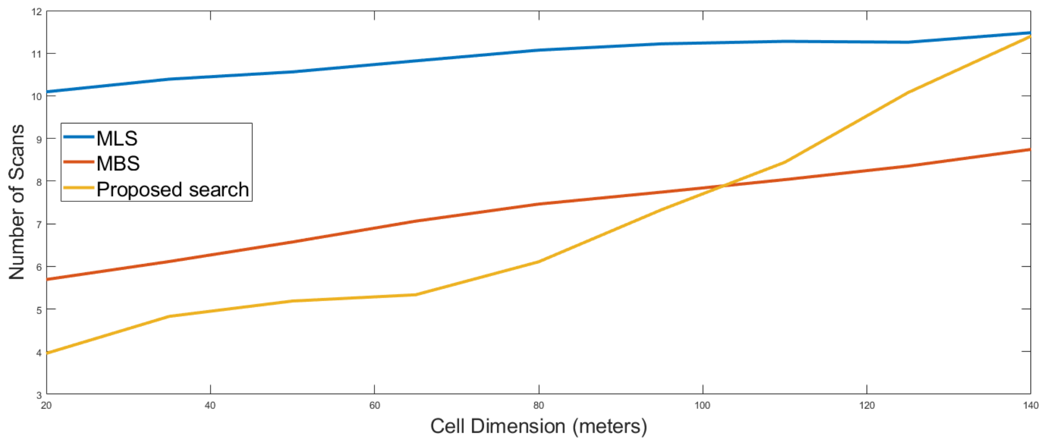

Figure 4.17: Mean number of scans vs cell dimension in the *random* scenario with uniform generation of UEs equipped with omni-directional antennas.

Figures 4.17, 4.18 and 4.19 show the results achieved with the uniform generation. In particular, Fig. 4.17 puts in evidence that our algorithm improves the performance with respect to the MLS and MBS approaches, when the cell size is lower than 100 m. After that, the proposed approach tends to deteriorate its performance while comparing to the other algorithms. This effect can be ascribed to the fact that this novel approach leverages on different HPBWs, and thus for larger distances testing with wider beam widths, which exhibit lower gains, might lead to misdetection and waste of time.

Concerning fig. 4.18 we can notice the same behaviour, even if relieved thanks to the beamforming gain at UE side which makes the channel less dependent on the gain at BS side.

Nevertheless, considering in particular the beamforming case in Fig, 4.18, our algorithm allows to enhance the MBS performance by a factor 10, as long

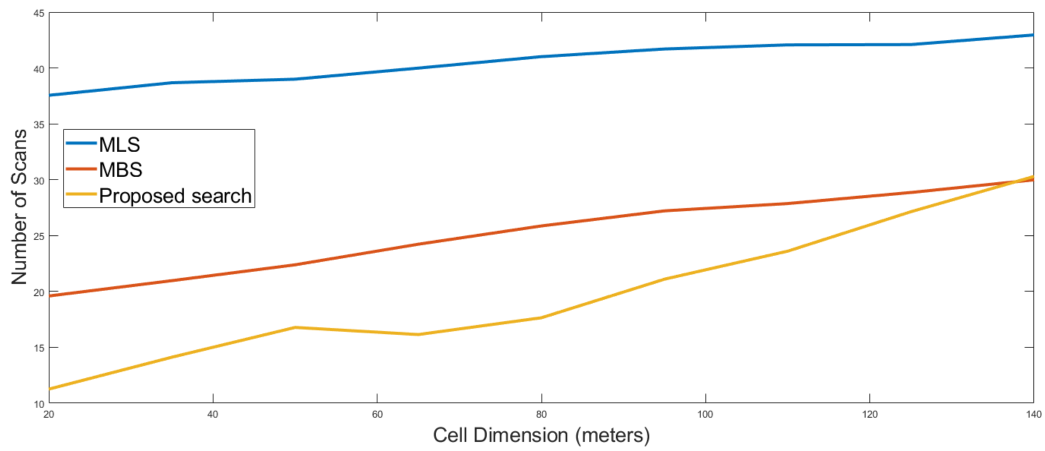

Figure 4.18: Mean number of scans vs cell dimension in the *random* scenario with uniform generation of UEs equipped with beamforming antennas.

as the cell is not too large. The possibility to use several HPBW lets the algorithm learn better the position of the obstacles with respect to the MBS.

The misdetection ratios in Fig. 4.19 and 4.22 show a trend similar to the previous one, but in this case the omnidirectional and the beamforming curves are closer. This is due to the increase of the gain in the BS, which permits to easily cover the whole cell. This means that the gain at UE side in less relevant than in the preceding simulations.

Summarizing, it has been shown that the use of an algorithm which leverages on both a memory and a multi codebook system can considerably decrease the IA delay without the support of a dedicated control channel.

Finally, we investigate the improvement obtained using the proposed UE approach. The considered accuracy of the GPS is the same as in Sec. 4.4, while error in the orientation estimation is set to $\sigma_N = 8°$.

Figures 4.23 and 4.24 show the results obtained when the UE is assumed to be capable to steer its beam towards four different sectors and to access an online *database*, as detailed in Sec. 3.5.2. Indeed, the improvement carried out by the *database* at the UE side is not remarkable, since it leads to decrease the number of scans in average only by 1 with respect to the memoryless UE approach. This effect comes from the following reason: assuming that the BS steers its beam towards the correct direction, the memoryless UE needs on average only 2-3 scans to find the best configuration, which is already well performing.

Thus, in case UEs with more complex antennas are considered (i.e., more steering directions for the UE), the improvement is expected to become more evident.

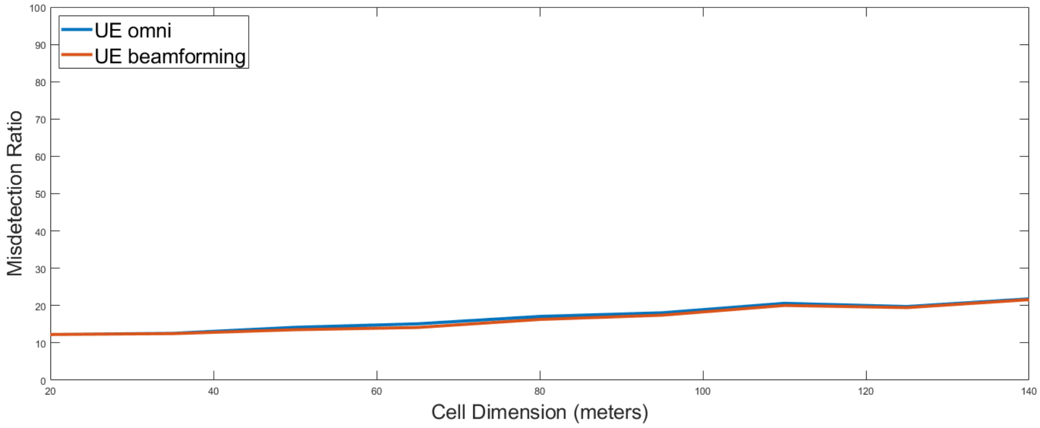

Figure 4.19: Misdetection ratio vs cell dimension in the *random* scenario with UEs equipped with beamforming antennas vs UEs equipped with omni-directional antennas. This curve has been obtained with the MLS approach with a HPBW = 15°.

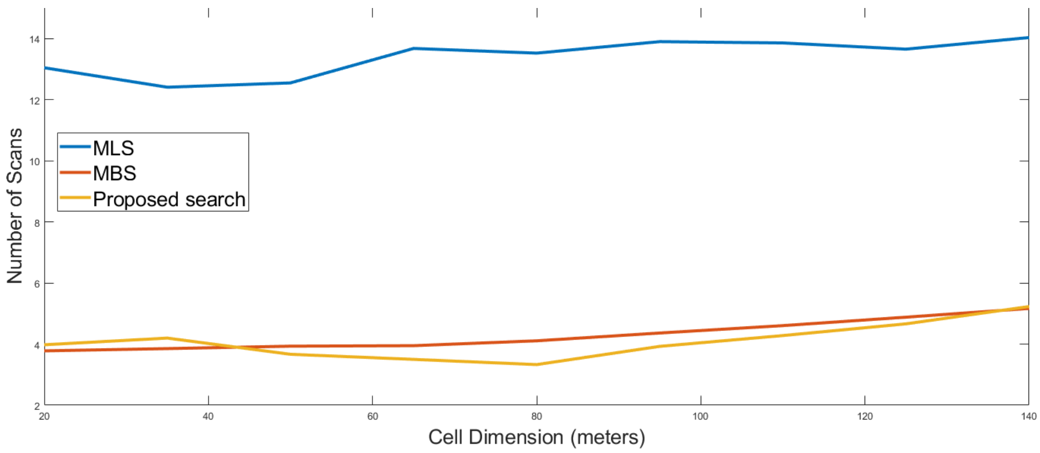

Figure 4.20: Mean number of scans vs cell dimension in the *random* scenario with non-uniform generation of UEs equipped with omni-directional antennas.

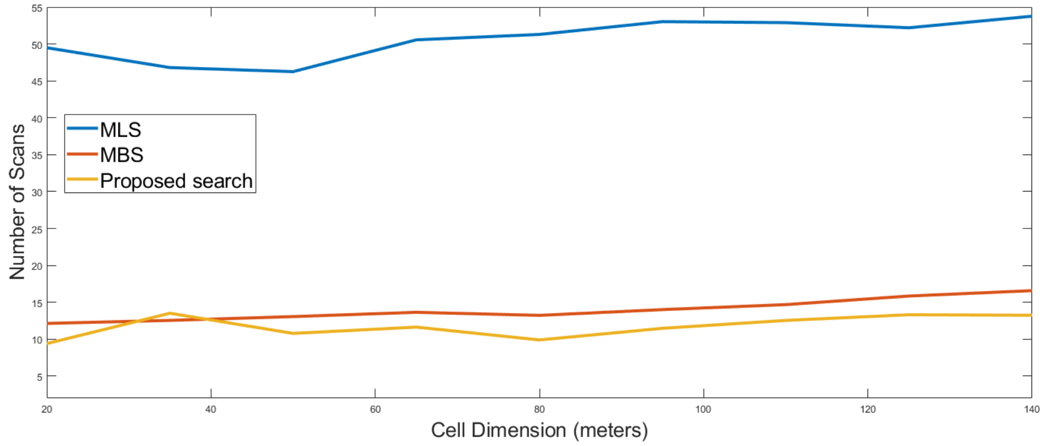

Figure 4.21: Mean number of scans vs cell dimension in the *random* scenario with non-uniform generation of UEs equipped with beamforming antennas.

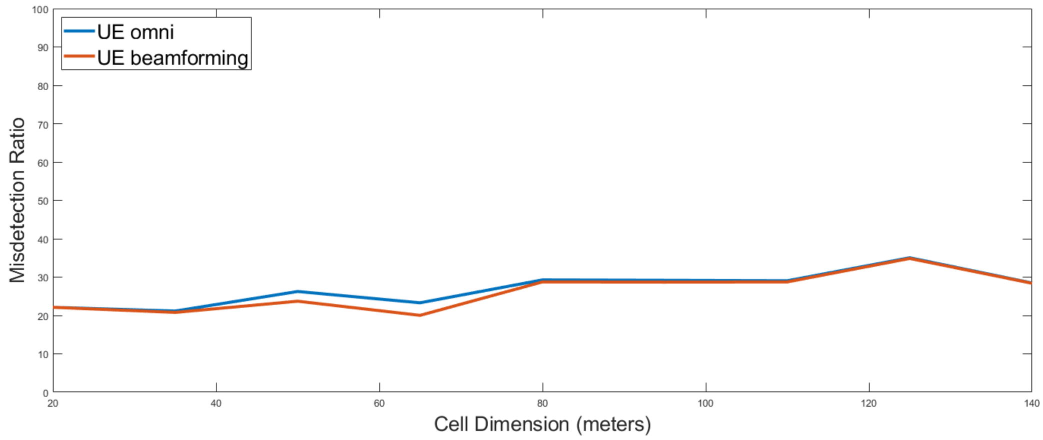

Figure 4.22: Misdetection ratio vs cell dimension in the *random* scenario with UEs equipped with beamforming antennas vs UEs equipped with omnidirectional antennas. This curve has been obtained with the MLS approach with a HPBW = 15° and non-uniform distribution of the UEs.

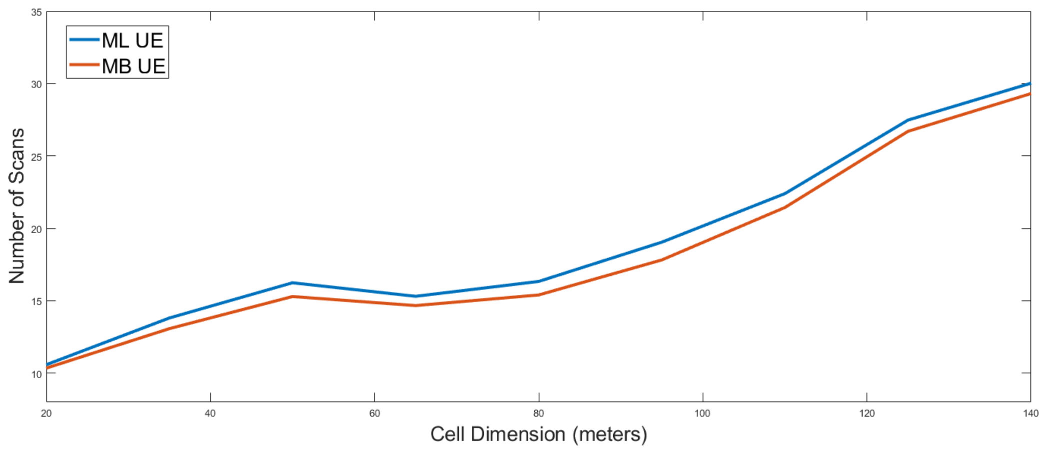

Figure 4.23: Mean number of scans vs cell dimension in the *random* scenario with uniform generation of UEs. The curves show the comparison between the memoryless and the memory-based algorithm at UE side.

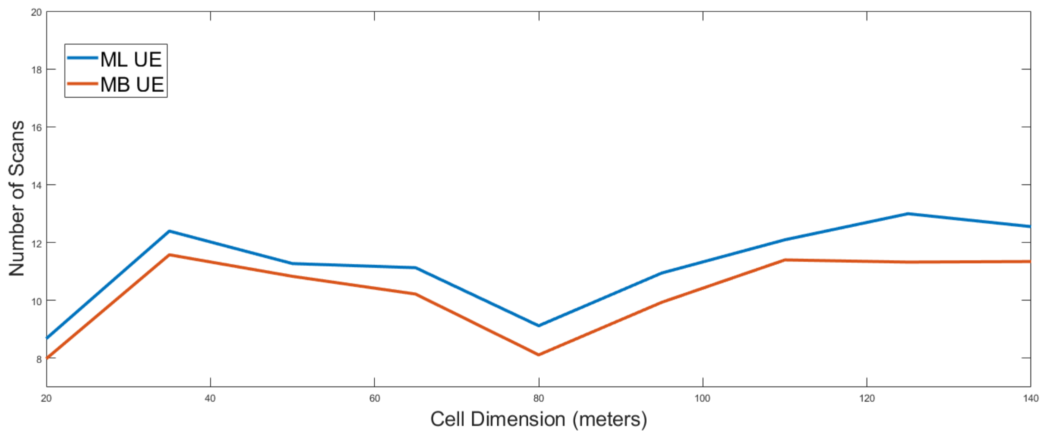

Figure 4.24: Mean number of scans vs cell dimension in the *random* scenario with non-uniform generation of UEs. The curves show the comparison between the memoryless and the memory-based algorithm at UE side.

Conclusions

The standardization of the 5G of wireless mobile systems represents one of the most important challenges of these years. Considering the different technologies areas in which 5G is involved, satisfying the several requirements implies a detailed study on each aspect of the system. In this document we have focused especially in the IA phase, primarily by studying the SOTA approaches considering both SA and NSA algorithms. In particular, it has emerged that SA algorithms usually consider statistical realization of the channels, which are not the most appropriate tool to evaluate a memory-based system because of they not dependence on user position. Moreover, the SA approaches which leverage on a memory-based system do not rely also on several HPBWs at BS side and usually neglect the UE to improve the IA procedure. Thus, we have designed a novel approach which leverages at BS side on a *knowledge database* that includes information about the detected UEs per sector with the adopted HPBW, and at UE side on the availability of information shared among previous detected UEs. Finally, we have developed a simulator based on a RT channel, in order to compare the algorithms.

The results we have obtained show that, first of all the mmWave communications are not straightforward to manage. In particular we have demonstrated that in most cases only LOS UEs can establish a communication link with the BS, while NLOS UEs are often unreachable. After that, we have proved that the memory is a key parameter for the IA techniques: the use of a memory-based system at BS and UE side allows to significantly reduce the *average discovery time*. Moreover, with our novel approach we have demonstrated that the use at BS side of a *knowledge database*, permits to notably enhance the performances with respect to the SA SOTA approaches. On the UE side, since we have considered only 4 steering directions, using a *database* based on the sharing of information with others UEs does not leads to a remarkable performance with respect to a memoryless UE implementation.

Future works at BS side might consider a larger number of HPBWs configurations, in order to evaluate whether a further performance improvement of the proposed algorithm can be attained. Moreover, it would be advisable, whenever a UE is detected by the BS with a HPBW, to increase in the *knowledge database* only the cells of the row associate to its received power, instead of the whole cells in the configuration. This would permit to discriminate the UEs with different received powers detected with a certain HPBW. Furthermore, it could be interesting to adapt the novel approach to a multi BSs scenario, where the BSs are able to share each others the *knowledge database* with the purpose to further decrease the *average discovery time*. On the other hand, concerning the UE side of the proposed approach, further tests should be conducted considering a HPBW less than 90°, in order to evaluate possible additional improvements even though that would require a more precise estimation of UE orientation which could be challenging. In perspective, it would be interesting to investigate the issue of IA in future cell-free networks that are under investigation for beyond 5G systems.

Ringraziamenti

Ci siamo, questo percorso di studi é terminato, e con esso termina una parte della mia vita. Arrivato alla fine in parte sono stanco, perché comunque questa tesi é stata veramente difficile da scrivere e terminare in maniera dignitosa, ma soprattutto mi sento emozionato. In tutti questi bellissimi anni di Universitá (si bellissimi, anche se spesso ho maledetto il giorno in cui mi sono iscritto ad ingegneria), sono sempre stato sicuro di quello che mi sarebbe accaduto il giorno dopo: sarei andato a lezione, oppure avrei avuto degli esami. Ma adesso devo affrontare quello che verrá dopo, e questo é veramente eccitante. Ho l'oblio davanti e va bene cosí.

Dopo il breve flusso di coscienza iniziale sará meglio ringraziare qualcuno visto il titolo di questo capitolo. In modo molto scontato ringrazio ovviamente i miei genitori che hanno creduto in me anche se non sono sempre stato un gran studioso, ma evidentemente loro sapevano che sotto sotto lo ero. E poi ringrazio tutti i miei amici che sono sempre disposti a bersi una birra con me e ascoltarmi durante i miei vaneggiamenti.

Un grandissimo ringraziamento va a Francesco Guidi e al Prof. Davide Dardari che mi hanno seguito tantissimo durante tutta questa tesi e che con tanta pazienza hanno corretto tutti i miei errori ed orrori (di inglese e non).

Non voglio dire altro che il tempo stringe e io adesso voglio andare a letto. Buonanotte.

List of Tables

List of Figures

Bibliography

[1] A. Osseiran, F. Boccardi, V. Braun, K. Kusume, P. Marsch, M. Maternia, O. Queseth, M. Schellmann, H. Schotten, H. Taoka, H. Tullberg, M. A. Uusitalo, B. Timus, and M. Fallgren, "Scenarios for 5G mobile and wireless communications: the vision of the metis project," *IEEE Communications Magazine*, vol. 52, no. 5, pp. 26–35, May 2014.

[2] M. Giordani, M. Mezzavilla, and M. Zorzi, "Initial access in 5G mmwave cellular networks," *IEEE Communications Magazine*, vol. 54, no. 11, pp. 40–47, November 2016.

[3] S. Rangan, T. S. Rappaport, and E. Erkip, "Millimeter-wave cellular wireless networks: Potentials and challenges," *Proceedings of the IEEE*, vol. 102, no. 3, pp. 366–385, March 2014.

[4] L. Wei, R. Q. Hu, Y. Qian, and G. Wu, "Key elements to enable millimeter wave communications for 5g wireless systems," *IEEE Wireless Communications*, vol. 21, no. 6, pp. 136–143, December 2014.

[5] "What are small cells in 5G technology," https://www.rfpage.com/what-are-small-cells-in-5g-technology/, updated: September 2018.

[6] M. Wang, Y. Li, H. Zou, M. Peng, and G. Yang, "Compact MIMO antenna for 5G portable device using simple neutralization line structures," in *2018 IEEE International Symposium on Antennas and Propagation USNC/URSI National Radio Science Meeting*, July 2018, pp. 37–38.

[7] W. Jiang, Y. Liu, Y. Cui, B. Wang, and S. Gong, "Compact wide-band MIMO antenna with high port isolation," in *12th European Conference on Antennas and Propagation (EuCAP 2018)*, April 2018, pp. 1–3.

[8] S. Syedakbar, S. Ramesh, and J. Deepa, "Ultra wide band monopole planar MIMO antenna for portable devices," in *2017 IEEE International Conference on Electrical, Instrumentation and Communication Engineering (ICEICE)*, April 2017, pp. 1–4.

[9] "Radio access networking challenges towards 2030." https://www.itu.int/en/ITU-T/Workshops-and-Seminars/201810/Documents/Matt_Latva-aho_Presentation.pdf.

[10] electronic component news (ECN), "Fact or fiction: What's real in 5G new radio," https://www.ecnmag.com/article/2018/05/fact-or-fiction-whats-real-5g-new-radio, october 2018.

[11] M. R. Akdeniz, Y. Liu, M. K. Samimi, S. Sun, S. Rangan, T. S. Rappaport, and E. Erkip, "Millimeter wave channel modeling and cellular capacity evaluation," *IEEE Journal on Selected Areas in Communications*, vol. 32, no. 6, pp. 1164–1179, June 2014.

[12] "FP7-ICT-608637 MiWEBA project deliverable D5.1 - Channel modeling and characterization," http://www.miweba.eu/wp-content/uploads/2014/07/MiWEBA_D5.1_v1.01.pdf, June 2014.

[13] I. Filippini, V. Sciancalepore, F. Devoti, and A. Capone, "Fast cell discovery in mm-wave 5G networks with context information," *IEEE Transactions on Mobile Computing*, vol. 17, no. 7, pp. 1538–1552, July 2018.

[14] M. Giordani, M. Mezzavilla, C. N. Barati, S. Rangan, and M. Zorzi, "Comparative analysis of initial access techniques in 5G mmwave cellular networks," in *2016 Annual Conference on Information Science and Systems (CISS)*, March 2016, pp. 268–273.

[15] "Initial access - mmwave networking group," http://mmwave.dei.unipd.it/research/initial-access/.

[16] R. Parada and M. Zorzi, "Cell discovery based on historical user's location in mmwave 5G," in *European Wireless 2017; 23th European Wireless Conference*, May 2017, pp. 1–6.

[17] H. Soleimani, R. Parada, S. Tomasin, and M. Zorzi, "Statistical approaches for initial access in mmwave 5G systems," in *European Wireless 2018; 24th European Wireless Conference*, May 2018, pp. 1–6.

[18] Y. Qi and M. Nekovee, "Coordinated initial access in millimetre wave standalone networks," in *2016 IEEE Conference on Computer Communications Workshops (INFOCOM WKSHPS)*, April 2016, pp. 59–64.

[19] F. Devoti, I. Filippini, and A. Capone, "Mm-wave initial access: A context information overview," in *2018 IEEE 19th International Symposium on "A World of Wireless, Mobile and Multimedia Networks" (WoWMoM)*, June 2018, pp. 1–9.

[20] R. E. Rezagah, H. Shimodaira, G. K. Tran, K. Sakaguchi, and S. Nanba, "Cell discovery in 5G hetnets using location-based cell selection," in *2015 IEEE Conference on Standards for Communications and Networking (CSCN)*, Oct 2015, pp. 137–142.

[21] "Chinadaily.com.cn: A bird's-eye view of new york city," http://www.chinadaily.com.cn/world/2015-07/09/content_21228787_2.htm, updated: 2015-07-09 08:09.

[22] R. J. Weiler, W. Keusgen, A. Maltsev, T. Kühne, A. Pudeyev, L. Xian, J. Kim, and M. Peter, "Millimeter-wave outdoor access shadowing mitigation using beamforming arrays," in *2016 10th European Conference on Antennas and Propagation (EuCAP)*, April 2016, pp. 1–5.

[23] "Federal communications commission: Millimeter wave propagation: Spectrum management implications," https://transition.fcc.gov/Bureaus/Engineering_Technology/Documents/bulletins/oet70/oet70a.pdf, updated: July 1997.

[24] "gps accuracy," https://www.gps.gov/systems/gps/performance/accuracy/.